

Localization landscape for interacting Bose gases in one-dimensional speckle potentials

Filippo Stellin,^{1,*} Marcel Filoche,^{2,†} and Frédéric Dias^{1,3,‡}

¹*Université Paris-Saclay, CNRS, ENS Paris-Saclay, Centre Borelli, 91190, Gif-sur-Yvette, France.*

²*Laboratoire de Physique de la Matière Condensée, École Polytechnique, CNRS, Institut Polytechnique de Paris, Palaiseau, 91120, France.*

³*School of Mathematics and Statistics, University College Dublin, Belfield, Dublin 4, Ireland.*

(Dated: August 23, 2022)

While the properties and the shape of the ground state of a gas of ultracold bosons are well understood in harmonic potentials, they remain for a large part unknown in the case of random potentials. Here, we use the localization-landscape (LL) theory to study the properties of the solutions of the Gross-Pitaevskii equation (GPE) in one-dimensional (1D) speckle potentials. In the cases of intermediate and strongly attractive interactions, we find an approximate relation which allows to evaluate the disorder-averaged localization length from the nonlinear coefficient of the GPE. For weakly repulsive interactions, we illustrate that the ground state ψ_0 of the quasi-1D GPE can be understood as a superposition of a finite number of single-particle states. For intermediate repulsive interactions, we show numerically that, in the smoothing regime, ψ_0 can be predicted using a Thomas-Fermi-like approach involving the effective potential, which is given by the reciprocal of the LL. Moreover, we show that, in the Lifshitz glass phase, the particle density and the chemical potential can be well estimated by means of the LL. Our approach can be applied for any random potential endowed with finite-range correlations and can be generalized to higher-dimensional systems.

I INTRODUCTION

Cold atom experiments are a remarkable platform to explore quantum theories and to test open questions in condensed matter physics. The modern developments in cooling and trapping techniques [1] have enabled to achieve Bose-Einstein condensation of matter waves [2, 3], thus opening the possibility to study their behavior in random optical potentials [4–7]. Bose-Einstein condensates, occurring in dilute samples and at very low temperature, of the order of tens of nK, are characterized by the macroscopic occupation of the ground state of the gas, described by a highly coherent and fully symmetric wavefunction. In the absence of interactions among atoms, the interference between the multiple scattering paths of an initially traveling particle can completely inhibit its diffusion, eventually leading to an exponential localization of the wavefunction [8–10]. This phenomenon, known as *Anderson localization*, has been actually observed [4–6, 11] and theoretically studied [12–15] with matter waves in different settings during the past 15 years.

The presence of interactions between atoms can significantly modify this picture. The study of the interplay between an external quenched disorder and an interacting Bose gas has motivated many theoretical [16–20] and experimental works [21–27]. The many-body interactions make computations of the many-particle states

incredibly much harder. However, by treating the interactions through a mean-field approach, one can reduce the dimensionality of the problem and model the gas by a one-particle nonlinear Schrödinger equation, also called the *Gross-Pitaevskii equation* (GPE) [28]. Theoretical investigations on these systems have been carried out from different perspectives, focusing on stationary states [29–33], excitations [34–37], dynamics [38–42], out-of-equilibrium physics [43–45], phase transitions [46–49], superfluidity [50] and solitons [51–53].

While the stationary states of the GPE in the weakly interacting limit [33, 46] and the Thomas-Fermi limit for repulsive interactions [29, 33] are quite well understood, we still lack to this day theoretical tools to tackle the intermediate regime and the strongly attractive limit.

In the case of strong repulsive interactions, it was shown that, for a chemical potential μ much larger than the standard deviation of the disorder V_0 , the kinetic term of the GPE can be neglected according to the Thomas-Fermi approximation [3, 54]. Hence, the macroscopic state at equilibrium follows the modulations of the random potential, as it was shown by considering speckle potentials [29, 31, 47] and Gaussian random potentials [19]. In correlated speckle potentials, Sanchez-Palencia pointed out that the stationary state becomes sensitive to the smoothed random potential [29] rather than the original one. This was predicted to take place when the correlation length σ is smaller than the healing length ξ , i.e. the maximum length of the spatial variations of the state ψ that contribute to the kinetic energy of the atoms [3]. Soon afterwards, Lugan *et al.* [46] proposed a schematic quantum-state diagram and predicted in the same geometry the occurrence of the Lifshitz glass phase for strong disorder and weakly repulsive interac-

* filippo.stellin@ens-paris-saclay.fr

† marcel.filoche@polytechnique.edu

‡ frederic.dias@ucd.ie

tions. In this regime, the Bose gas splits into fragments whose shapes are given by nonoverlapping single-particle (SP) states belonging to the Lifshitz tails of the integrated density of states (IDoS). Regime diagrams for the repulsive case were also built by Falco *et al.* [30, 32]. They examined random potentials with unbounded probability distributions and different correlation profiles, superimposed with harmonic potentials along all directions. Four different regimes were distinguished, based on the spatial behavior of the particle density: the harmonic, the Thomas-Fermi, the nonergodic and the fragmented ones. However, in the aforementioned studies the collective N -particle states were not computed explicitly, but estimates of the typical size of the atomic cloud or of its fragments were provided as functions of the characteristic lengths associated to the random potential and of the coefficient of the nonlinear term $g(N-1)$ of the GPE.

A numerical investigation of the ground state ψ_0 for weakly repulsive and attractive interactions was carried out in the work of Cheng *et al.* [33], who considered 1D speckle potentials and showed that, for weak interactions, the state remains exponentially localized with a localization length that increases for stationary solutions of the defocusing GPE, whereas it decreases for the focusing GPE.

The work presented here intends to fill the gap of knowledge between the noninteracting and the Thomas-Fermi regime as well as in the strongly attractive limit by exploiting the concept of localization landscape (LL) [55] which was initially introduced for the non-interacting problem. We exhibit analytic approximations of the many-particle state in 1D speckle potentials in several cases, and also contribute to unveil connections to the SP states which were previously analyzed merely in fully harmonic potentials [56, 57].

Our paper is structured as follows. In Sec. II we present the physical system, introducing the Gross-Pitaevskii equation, the features of the correlated random potential and the LL function used throughout the work. In the remaining sections, we investigate the regions in the interaction-disorder plane depicted in Fig. 1.

In Sec. III, we examine the attractive case and we derive a relation which accurately predicts the disorder-averaged localization length when the interaction energy is much higher than the mean value of the random potential (Sec. III A). In Sec. III B, we find that the aforementioned length monotonically decreases for increasing disorder strength.

Sec. IV is devoted to the case of repulsive interactions. Here the ground state of the GPE is displayed for a wide range of random potential amplitudes and nonlinear coefficients. In Sec. IV A 1, we prove that for weak interactions, the ground state of the GPE with speckle potentials can be predicted by an expansion over a finite number of (localized) SP states. We assess the quality of the LL approach by comparing those states, computed by exact diagonalization of the SP Hamiltonian, against the solutions of the eigenvalue problem restricted to the

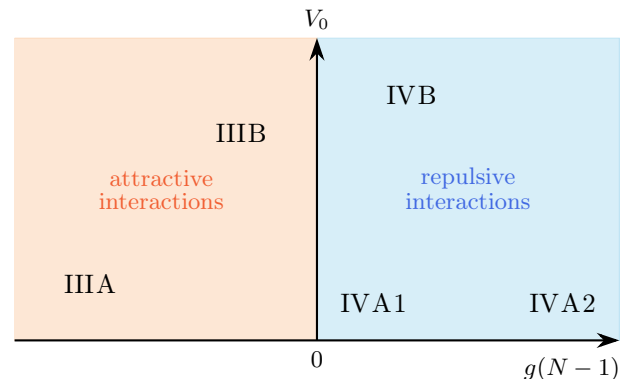


FIG. 1. Interaction-disorder diagram in which the numbers of the sections pinpoint the regions of the plane where the ground state of the GPE is examined.

regions of the lowest minima of the effective potential derived from the LL [58].

In Sec. IV A 2, we show that, for intermediate repulsive interactions, the LL-based effective potential sets the typical variation scale of the macroscopic wavefunction. We point out that the last mentioned quantity can be approximated using a Thomas-Fermi-like ansatz.

In Sec. IV B, we compute the ground state in a regime where it is given by a superposition of SP wavefunctions which do not spatially overlap with each other and whose energy lies in the Lifshitz tails of the IDoS. In this case, we show that the number of particles in each of the SP wavefunctions, occurring at the wells of the effective potential, are well predicted by the LL together with a relation derived by Luga *et al.* [46].

In Sec. V, we draw the conclusions and outline the possible perspectives of this work.

II THE LOCALIZATION LANDSCAPE OF THE GROSS-PITAEVSKII EQUATION

A The Gross-Pitaevskii equation

We consider an ultracold dilute Bose gas in which interaction events are *binary*, i.e. involve only two particles at a time, and are characterized by a length scale that is smaller than the de Broglie wavelength, so that the scattering events are dominated by s -wave processes. Under these conditions, the ground state of the many-particle system is given by the common wavefunction $\psi(\mathbf{r})$, normalized to unity, which obeys the Gross-Pitaevskii equation:

$$\left[-\frac{\hbar^2}{2m}\nabla^2 + V(\mathbf{r}) \right] \psi(\mathbf{r}) + \frac{4\pi\hbar^2 a_s}{m} (N-1) |\psi(\mathbf{r})|^2 \psi(\mathbf{r}) = \mu \psi(\mathbf{r}), \quad (1)$$

where a_s represents the s -wave scattering length. To ensure the validity of Eq. (1) for a quantum gas, a_s must satisfy a low-density assumption, $\langle \rho \rangle |a_s|^3 \ll 1$ [3], $\langle \rho \rangle = N \langle |\psi|^2 \rangle$ being the spatial average of the particle density. Moreover, one has to note that this nonlinear coupling can be experimentally tuned by means of Feshbach resonances [59]. By applying a tight harmonic confinement on one or two dimensions [29, 46], it is possible to assess the effect of disorder on the macroscopic wavefunction in low-dimensional quantum gases. In the following, we focus on potentials exhibiting a 1D disorder along Ox , which means that the total potential can be written as

$$V_{\text{tot}}(x, y, z) = V_R(x) + \frac{1}{2} m \omega_{\perp}^2 (y^2 + z^2), \quad (2)$$

where V_R is the 1D random potential and ω_{\perp} is the pulsation of the two-dimensional (2D) harmonic well in the directions y and z . Assuming that $\hbar \omega_{\perp}$ is much larger than the level spacing between two consecutive eigenvalues of the noninteracting 1D problem, the ground state of this potential can be factorized as

$$\psi_0(\mathbf{r}) = \psi_0(x) \phi_0^{(\text{ho})}(y, z), \quad (3)$$

where

$$\phi_0^{(\text{ho})}(y, z) = \sqrt{\frac{m \omega_{\perp}}{\pi \hbar}} \exp \left\{ -\frac{m \omega_{\perp}}{2 \hbar} (y^2 + z^2) \right\}, \quad (4)$$

is the ground state of the 2D harmonic oscillator in the (y, z) plane. The two wavefunctions ψ_0 and $\phi_0^{(\text{ho})}$ satisfy the normalization conditions $\int dx |\psi_0(x)|^2 = 1$ and $\int dy dz |\phi_0^{(\text{ho})}(y, z)|^2 = 1$, respectively. After integrating out the 2D harmonic wavefunction, one finds that ψ_0 obeys [29, 60]

$$\left[-\frac{\hbar^2}{2m} \frac{\partial^2}{\partial x^2} + V_R(x) + \hbar \omega_{\perp} + 2 \hbar \omega_{\perp} a_s (N-1) |\psi_0(x)|^2 \right] \psi_0(x) = \mu \psi_0(x). \quad (5)$$

The nonlinear coupling appearing in the last term of the Schrödinger operator is characterized hereafter by the constant

$$g := 2 \hbar \omega_{\perp} a_s. \quad (6)$$

The random potential V_R is a correlated speckle potential, typically engineered by exploiting the coupling between the atomic dipole moment and the electric field generated by shining coherent light on a diffusive plate [61]. Owing to the central limit theorem, both the real and the imaginary parts of the electric field in the observation point, for a high number of scattering events [62], follow a Gaussian probability distribution. This leads to the formation of the speckle pattern where the probability distribution of the random potential am-

plitude is given by a Rayleigh law,

$$P(V_R) = \frac{\Theta_H(V_R/V_0)}{V_0} e^{-V_R/V_0}, \quad (7)$$

$\Theta_H(x)$ being the Heaviside step function and V_0 the disorder strength. V_0 is inversely proportional to the detuning between the laser frequency and the atomic transition frequency [59]. It is positive for blue-detuned speckles or negative for red-detuned ones. The spatial correlation profile $C(x)$ of the potential is chosen to be Gaussian, as one of those used in Ref. [14]:

$$C(x) := \overline{[V_R(0) - V_0][V_R(x) - V_0]} = V_0^2 e^{-\frac{x^2}{2\sigma^2}}, \quad (8)$$

in which σ denotes the correlation length. The symbol $\overline{\cdot}$ indicates the ensemble average over all configurations of the disordered potential.

For a 1D domain of length L ($-L/2 \leq x \leq L/2$), the energy associated to the ground state of the GPE (5) is given by [3]

$$E_0 = \int_{-L/2}^{L/2} \left[\frac{\hbar^2}{2m} \left| \frac{d\psi_0(x)}{dx} \right|^2 + (V_R(x) + \hbar \omega_{\perp}) |\psi_0(x)|^2 + \frac{g(N-1)}{2} |\psi_0(x)|^4 \right] dx, \quad (9)$$

whereas the corresponding chemical potential reads

$$\mu = E_0 + \frac{g(N-1)}{2} \int_{-L/2}^{L/2} |\psi_0(x)|^4 dx. \quad (10)$$

B The localization landscape

In order to understand the behavior of the 1D ground state ψ_0 of the GPE, we start from the SP Hamiltonian H^{SP} :

$$H^{\text{SP}} := -\frac{\hbar^2}{2m} \frac{\partial^2}{\partial x^2} + \hbar \omega_{\perp} + V_R(x). \quad (11)$$

The localization landscape, introduced in Ref. [55], is then defined as the solution to

$$H^{\text{SP}} u = 1. \quad (12)$$

In this article, we choose to impose the Dirichlet boundary conditions on the LL (but they could be as well periodic, since they play no real role on localization effects):

$$u(x)|_{x=\pm \frac{L}{2}} = 0. \quad (13)$$

By decomposing an eigenstate ψ^{SP} of H^{SP} as $\psi^{\text{SP}} = u \varphi^{\text{SP}}$, where φ^{SP} is an auxiliary function and using (12),

the time-independent Schrödinger equation $H^{\text{SP}}\psi^{\text{SP}} = E^{\text{SP}}\psi^{\text{SP}}$ can be rewritten as

$$-\frac{\hbar^2}{2m} \left[\frac{1}{u^2} \frac{\partial}{\partial x} \left(u^2 \frac{\partial}{\partial x} \varphi^{\text{SP}} \right) \right] + \frac{1}{u} \varphi^{\text{SP}} = E^{\text{SP}} \varphi^{\text{SP}}. \quad (14)$$

We see that the auxiliary function obeys a Schrödinger-like equation in which the Laplacian is replaced by a slightly more complicated elliptic operator whereas the original potential $V(x) := V_R(x) + \hbar\omega_\perp$ is substituted by the effective potential $V_{\text{LL}}(x)$, defined as

$$V_{\text{LL}}(x) := u(x)^{-1}. \quad (15)$$

It has been shown that this rewriting of the Schrödinger equation allows one to view the exponential localization (Anderson localization) of the lowest lying-states as a semiclassical confinement process in the smoother disordered potential V_{LL} [55, 58]. The LL also permits to identify the position of those states without solving the full eigenvalue problem [63] and accounts for the behavior of the tails of the integrated density of states [64].

For the sake of simplicity, in the following treatment all quantities will be nondimensionalized, based on the units of the transverse harmonic oscillator. Hence, the lengths will be expressed in units of the oscillator length $l_\perp := \sqrt{\frac{\hbar}{m\omega_\perp}}$ and the energies in units of the transverse zero-point energy $E_{0,\perp} := \hbar\omega_\perp$.

C Numerical methods

For computing the ground state of the GPE, we adopt a Crank-Nicolson method with imaginary time which was introduced by Muruganandam and Adhikari [65]. This method is based on the iteration of (imaginary) time-evolution steps. The time-evolution process is performed by first considering only the potential and the nonlinear terms, then by involving the kinetic term of the GPE (5) which is discretized to the second order in the lattice parameter a . The initial wavefunction is taken to correspond to the ground state of the noninteracting Hamiltonian H^{SP} and it is reckoned by solving the eigenvalue problem

$$H^{\text{SP}}\psi_i^{\text{SP}} = E_i^{\text{SP}}\psi_i^{\text{SP}}, \quad (16)$$

in an interval of the domain. This interval, which is identified as proposed in Ref. [63], is pinpointed as the connected region Ω_{LL} containing the absolute minimum $V_{\text{LL},\text{min}}$ of the effective potential V_{LL} , such that $V_{\text{LL}}(x) \leq (1 + d/2)V_{\text{LL},\text{min}}$. This condition guarantees that the region is deep enough to hold a localized eigenfunction. The ψ_0^{SP} in Ω_{LL} is numerically computed by using a divide-and-conquer algorithm for the diagonalization of symmetric matrices. Starting from this SP state, the evaluation of ψ_0 proceeds as detailed in Ref. [65], with an intermediate solution at the subsequent time-step com-

puted by retaining only the kinetic term. The potential as well as the nonlinear term are then introduced in a first-order time integration with the aim of achieving the complete evolution after a single time-step. The bipartite procedure thus outlined is repeated $N_{\text{pas}} \sim 10^5$ times, a value which can be varied to check the convergence of the result. The stationary state of the GPE thus obtained vanishes at the boundaries of the 1D domain.

Besides, in the computation of the energy associated to ψ_0 and of the corresponding chemical potential, both the integrations in Eqs (9) and (10) are performed numerically, taking advantage of Cavalieri-Simpson's 3/8 rule [66].

In addition, the landscape function is calculated from Eq. (12) by using a finite-element method and applying the boundary conditions shown in Eq. (13).

In order to assess the accuracy of some of the approaches based on the LL, the lowest-lying SP eigenstates $\{\psi_i^{\text{SP}}\}$ and their eigen-energies $\{E_i^{\text{SP}}\}$ are also computed by exact diagonalization of the SP Hamiltonian in Eq. (11), with Dirichlet boundary conditions.

III ATTRACTIVE INTERACTIONS

The spatial behavior of the 1D ground state ψ_0 of the GPE is first investigated in the case of attractive interactions. To this end, in this section we examine the effect of both interactions and disorder on ψ_0 . In the numerical simulations, we deal with samples of $N = 2.67 \times 10^4$ atoms as in Ref. [67] with the same transverse-confinement length as the one of the harmonic potential used in that experiment. For the one-dimensional random potential, which is absent in Ref. [67], we consider a blue-detuned speckle potential endowed with a correlation length $\sigma = 0.09$ as in Ref. [4].

A Exploring the strength of the interactions

As it was first pointed out by Cheng and Adhikari in Ref. [33], for attractive interactions the ground state of the GPE is localized in space and its tails decay exponentially. In finite quasi-1D systems, the left and the right tails do not exhibit exactly the same decay, which means that the modulus of the wavefunction can be approximated by:

$$|\psi_0(x)| \approx c_a \begin{cases} e^{\frac{(x-x_0)}{\lambda_L}} & -\frac{L}{2} \leq x < x_0 \\ 1 & x = x_0 \\ e^{\frac{-(x-x_0)}{\lambda_R}} & x_0 < x \leq \frac{L}{2} \end{cases}, \quad (17)$$

where x_0 is the localization center, and λ_L and λ_R denote the left and the right localization length, respectively. Moreover, in Eq. (17), c_a represents the normalization coefficient. In large 1D domains ($L \gg \lambda_L, \lambda_R$),

the two localization lengths become statistically identical, since the disorder is isotropic and identically independently distributed. Under these conditions, by taking $\lambda_R = \lambda_L =: \lambda$ and plugging Eq. (17) into the definition of the chemical potential (10), one gets an approximate expression for μ in terms of the parameters of the GPE, following the procedure detailed in App. A. This relation reads:

$$\mu[\lambda, V_0, g(N-1)] = \frac{1}{2\lambda^2} + 1 + V_0 + \frac{g(N-1)}{2\lambda}. \quad (18)$$

Since the system under consideration is self-averaging [68], the Lyapunov exponent, i.e. the inverse of the localization length [69] associated to the wave-function ψ_0 , in a sufficiently large domain becomes equal to the average over the disorder realizations. The expression in the right-hand side of Eq. (18) can be therefore regarded as independent of the configuration of the random potential, so one can approximate the localization length λ with its mean value $\bar{\lambda}$ over all configurations.

The relation between the average localization length and the nonlinear coefficient can be then found by minimizing the chemical potential with respect to λ , thus obtaining:

$$\bar{\lambda} = -\frac{2}{g(N-1)}. \quad (19)$$

Plugging the right-hand side of Eq. (19) into Eq. (18), the chemical potential takes the form:

$$\mu = V_0 + 1 - \frac{g^2(N-1)^2}{8}. \quad (20)$$

By starting from the parameters detailed at the beginning of the present section, we numerically determine the ground state ψ_0 by varying only the coefficient of the nonlinear term, $g(N-1)$, from -1 to $-1,000$, by multiplicative steps of 10. In addition, we compute the ground state for vanishing interactions. The speckle potential is endowed with a mean value $V_0 = 2.45 =: V_0^{e,a}$ as in Ref. [4], and the potentials V and V_{LL} for a single disorder configuration are plotted in Fig. 2a by the orange and the blue solid lines respectively. The wavefunctions are represented in Fig. 2b as the solid curves, of which the ones for $g(N-1) = 0$ and for $g(N-1) = -1$ nearly overlap.

In accordance with the predictions in Ref. [63], we find that ψ_0 for $g(N-1) = 0$ is significant only in the region of the absolute minimum of the effective potential V_{LL} , occurring at $x = 12.2$ for the realization displayed in Fig. 2a. As $|gN|$ is increased, the wavefunction ψ_0 becomes more tightly localized but its absolute maximum shifts only slightly, as clarified in Fig. 2b, remaining in the interval between the local maxima of V_{LL} in $x = 10.9$ and $x = 14.4$. Increasingly attractive interactions hence lead to a narrowing of the ground state ψ_0 in space.

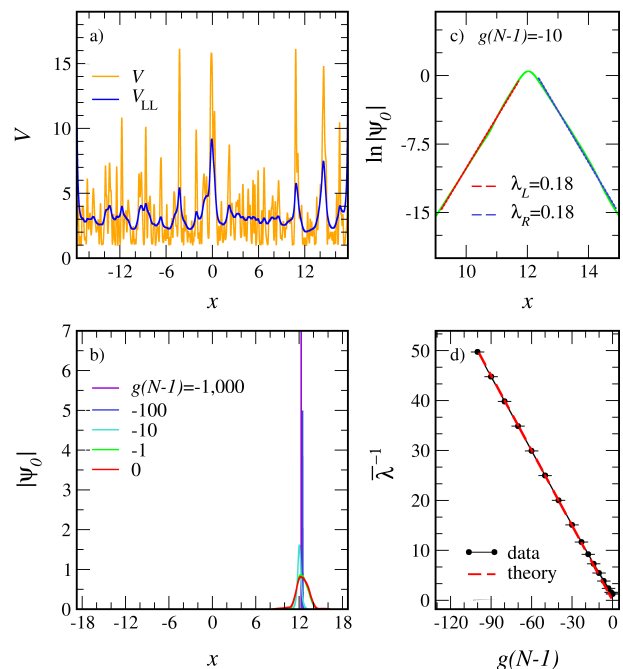


FIG. 2. Variable attractive interactions in a blue-detuned speckle potential with mean $V_0 = 2.45$ and correlation length $\sigma = 0.09$, in a domain of length $L = 40,000a$, where $a = 8.8 \cdot 10^{-4}$. Panel (a): total potential V (orange solid line) and effective potential V_{LL} (dark-blue solid line) along Ox . Panel (b): moduli of the ground states of the GPE (Eq. (5)) for five different values of the coefficient of the nonlinear term, ranging from $g(N-1) = -1,000$ to $g(N-1) = 0$ (solid lines). Panel (c): logarithm of the wavefunction represented in light green in Panel (b), with linear regressions on its left and right tails (red and blue dashed lines, respectively). Panel (d): the inverse of numerical mean value of the localization length $\bar{\lambda}$ (black line with filled circles), with errorbars and standard deviations (gray shaded area), and theoretical value of $\bar{\lambda}^{-1}$ (red long-dashed line), based on Eq. (19).

In Fig. 2c, the logarithm of the absolute value of ψ_0 is plotted for $g(N-1) = -10$ in order to show the agreement between the numerical wavefunction and the approximation in Eq. (17). In this example, the absolute difference between λ_R and λ_L amounts to 10^{-4} . This is consistent with our approximation of a unique localization length on both sides of ψ_0 .

In Fig. 2d, the disorder-averaged localization length $\bar{\lambda}$ is displayed as a function of the nonlinear coefficient, whereas the error bars refer to the error on the mean values. Besides, the very thin gray shaded area includes the values of the localization length that differ from $\bar{\lambda}$ by less than one standard deviation. Since the systems analyzed, of size $L = 40,000a$, are almost self-averaging, only 50 realizations of the random potential are needed to achieve an uncertainty lower than 3% with respect to $\bar{\lambda}$. The numerical data, represented by the black circles, agree well for strong interaction with the theoretical data based on Eq. (19), plotted as the long-dashed red line in

Fig. 2d. In particular, for $g(N-1) \lesssim -10$, the discrepancies between the predictions and the numerical results amount to 2% on average. However, for weak attractive interactions, Eq. (19) fails to predict $\bar{\lambda}$ since the contribution of the disorder exceeds the one of interactions. The approximation carried out for the contribution of the speckle potential to the right-hand side of Eq. (18), illustrated in App. A, proves in fact to be too coarse for $-3 \leq g(N-1) \leq 0$.

The appropriateness of Eq. (19) for intermediate and strongly attractive interactions appears to be consistent with the known result [54, 70] obtained in the absence of disorder. Under these conditions, i.e. for $V_0 = 0$ and for $L \gg -2/g(N-1)$, the ground state of the GPE indeed reads:

$$\psi_0(x) = \frac{\text{sech}(x/\zeta)}{\sqrt{2\zeta}}, \quad (21)$$

where the characteristic length ζ is

$$\zeta := \frac{2}{|g|(N-1)}. \quad (22)$$

The tails of ψ_0 in Eq. (21) thus decay exponentially in space with a typical length which coincides with the disorder-averaged localization length in Eq. (19).

We also remark that, since the wavefunction on the transverse directions is assumed to occupy the ground state of the 2D harmonic oscillator, the simulations on ψ_0 do not predict any collapse of the ground state for strongly attractive interactions, in accordance with the case of square-well potentials [71]. Indeed, for higher-dimensional configurations, we expect the existence of a threshold in the nonlinear coefficient above which no stationary solution exists, as it was predicted in harmonic potentials [72]. Compared to the study presented in Ref. [33], the localization length is here averaged over the disorder realizations and computed for a much wider range of nonlinear coefficients, thus allowing to unveil the relation between the disorder-averaged localization length $\bar{\lambda}$ and the nonlinear coefficient $g(N-1)$.

B Exploring the mean disorder strength

Let us now examine how the behavior of the ground state ψ_0 of the GPE is affected if only the mean value of the speckle potential is varied.

In Fig. 3a we dwell upon a single realization of the speckle potential, which is computed for three different mean values V_0 ranging from $0.1V_0^{e,a}$ to $10V_0^{e,a}$, by multiplicative steps of 10. The effective potentials are represented by the solid lines. For the sake of readability, the original potential is plotted only for $V_0 = 0.1V_0^{e,a}$ as the orange dashed line. In Fig. 3b the corresponding ground states of the GPE are represented by the solid lines of different colors and the quantities are computed by fixing the interaction to $g(N-1) = -1.5$, as in [67].

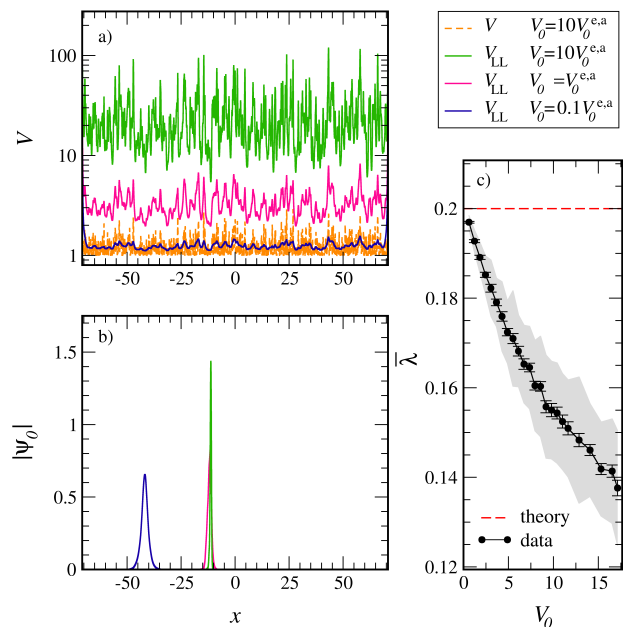


FIG. 3. Variable disorder parameter in attractively interacting Bose gases in blue-detuned speckle potentials with correlation length $\sigma = 0.09$ in domains of length $L = 40,000a$, where $a = 3.6 \cdot 10^{-3}$. Panel (a): effective potential V_{LL} for three different mean values ranging from $0.1V_0^{e,a}$ to $10V_0^{e,a}$ (solid lines). Total potential V for $V_0 = 0.1V_0^{e,a}$ (orange dashed line). Panel (b): ground state ψ_0 of the GPE with $g(N-1) = -1.5$ computed for the same values of V_0 as in Panel (a), represented by solid lines whose colors vary according to those of the effective potentials. Panel (c): disorder-averaged localization length $\bar{\lambda}$ (black solid line with filled circles), computed for $g(N-1) = -10$, with errorbars and standard deviation around $\bar{\lambda}$ (light-gray shaded region). Theoretical approximation based on Eq. (19) (red dashed line).

From the comparison between Figs. 3a and 3b, we notice that the wavefunctions possess a single maximum, located at the absolute minimum of the effective potential, which shifts from $x = -42$ to $x = -11$ as V_0 is increased within the aforementioned range. In Fig. 3c, the disorder-averaged localization length $\bar{\lambda}$ for $g(N-1) = -10$ is plotted as a function of the mean value of the random potential (the curve is computed for 90 configurations of V_R and the gray shaded area represents one standard deviation around it). As it can be inferred from Fig. 3, for $0.1V_0^{e,a} \leq V_0 \leq 5V_0^{e,a}$, $\bar{\lambda}$ monotonically decreases as the mean value of the speckle potential is raised, whereas the standard deviation increases.

Here, the theoretical approach introduced in Sec. III A is not able to account for this behavior since the approximation of the contribution of the random potential to μ , in Eq. (18), proves to be too coarse. In principle, we expect that this term should depend not only on the disorder parameter V_0 , but also on both the average localization length $\bar{\lambda}$ and the correlation length σ . Nevertheless, for decreasing disorder, the theoretical approximation in

Eq. (19), represented by the red dashed line in Fig. 3c, corresponds to the limit of the numerical data at low disorder strength. For instance, at $V_0 = 0.25V_0^{e,a}$, the relative discrepancy between the analytical and numerical data drops to 1%.

After having studied the dependence of the disorder-averaged localization length $\bar{\lambda}$ on the nonlinearity coefficient and on the disorder mean amplitude, we will now turn our attention to the case in which the GPE is defocusing.

IV REPULSIVE INTERACTIONS

Let us now investigate the case of repulsive interactions, considering a Bose gas with a s-wave scattering length $a_s = 0.004$ [73] in speckle potentials with a correlation length of $\sigma = 0.2$, as in the experiment of Billy *et al.* [4]. In this section we first investigate the behavior of the 1D ground state ψ_0 of the GPE as the nonlinear coefficient is varied, treating the regimes of weak interactions and intermediate or strong interactions separately. We later dwell on the shape and the properties of ψ_0 as the mean value V_0 of the random potential is varied, with a particular attention on the Lifshitz glass phase.

A Exploring the strength of the interactions

In order to provide an overview of the features of the ground state for repulsive interactions, we first plot it for $g(N-1) = 10^0, 10^1, \dots, 10^4$, considering a single realization of the random potential, characterized by a mean value $V_0 = 1.1 =: V_0^{e,r}$ and a correlation length $\sigma = 0.2$, as in Ref. [4]. Starting from these data, we represent the total potential V and V_{LL} in Fig. 4a and the wavefunctions obtained in the noninteracting case as well as for the aforementioned five different values of $g(N-1)$ above mentioned in Fig. 4b.

For increasing repulsive interactions, ψ_0 becomes significant in larger regions of the 1D domain, eventually spreading over the whole interval $[-L/2, L/2]$. At the same time, the amplitude of the oscillation of the wavefunction decreases as $g(N-1)$ is increased.

In the noninteracting case, ψ_0 is exponentially localized, in accordance with theoretical predictions [74] and experimental results [4] in 1D speckle potentials with short-range correlations. For the configuration displayed in Fig. 4a, the ground state in the red curve in Fig. 4b is localized at $x \approx 17$, which corresponds to the absolute minimum of the effective potential V_{LL} (thick black arrow in Fig. 4a), in agreement with the LL theory [63]. ψ_0 decays exponentially in space, following Eq. (17), and nonlinear regressions for $x < x_0$ and $x > x_0$ yield $\lambda_L = 0.959 \pm 0.001$ and $\lambda_R = 0.715 \pm 0.001$.

For $g(N-1) = 1$, the ground state is significant only in two disconnected regions, as displayed in Fig. 4b. This indicates that the bosons fall into three clusters

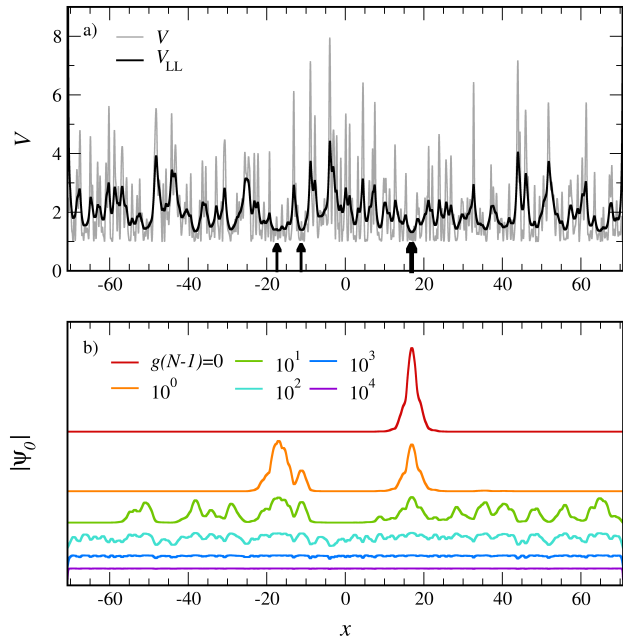


FIG. 4. Variable repulsive interactions. Panel (a): speckle potential V (grey solid line) with $V_0 = 1.1$ and $\sigma = 0.2$ and effective potential V_{LL} (black solid line) in a domain of length $L = 40,000a$, with lattice spacing $a = 0.0035$. The red arrow indicates the absolute minimum of V_{LL} , whereas the dark-orange arrows pinpoint the three next-to-lowest minima of V_{LL} . Panel (b): modulus of the ground state $|\psi_0|$ computed for different values of the nonlinear coefficient (solid lines): $g(N-1) = 0$ (red), $= 1$ (orange), $= 10$ (green), $= 100$ (turquoise), $= 1,000$ (blue), $= 10,000$ (violet). The base-lines of the wavefunctions are tilted in order to display more clearly the curves.

around the four lowest minima of the effective potential, pinpointed by the three black arrows in Fig. 4a. For $g(N-1) \lesssim 10$, the Bose gas is fragmented into multiple regions, but does not explore all the 1D domain. Unlike in the last mentioned case, as shown in Fig. 4b, for $100 \lesssim g(N-1) \lesssim 1,000$, ψ_0 spreads over all the lattice, with maxima and minima occurring approximately at the minima and maxima of the effective random potential V_{LL} , respectively. For instance, regarding the ground states for $g(N-1) = 100$ and $g(N-1) = 1000$ reported in Fig. 4b, the average distances between the local maxima (resp. minima) of ψ_0 and the closest local minima (resp. maxima) of V_{LL} amount to 0.16 and to 0.10 (resp. 0.13 and 0.05) in that order. Concomitantly, the same quantity computed with respect to the total potential V yields in those two cases 0.58 and 0.25 (resp. 0.63 and 0.27) respectively.

For $g(N-1) = 10^4$, the wavefunction follows the modulations of the original potential $V(x)$ and is well predicted

by the Thomas-Fermi approximation [29]:

$$|\psi_0^{\text{TF}}(x)| = \begin{cases} \sqrt{\frac{\mu - V(x)}{g(N-1)}} & \mu \geq V(x) \\ 0 & \mu < V(x) \end{cases}. \quad (23)$$

The superposition integral between the numerical wavefunction and the one in Thomas-Fermi approximation for the last-mentioned value of $g(N-1)$ amounts in fact to 1.000. In addition, the average distance between the minima (resp. maxima) of V and the maxima (resp. minima) of ψ_0 yields 0.12 (resp. 0.09) in this case. This approximation of the ground state, which does not involve the computation of the LL, is valid since the healing length $\xi := 1/\sqrt{2\mu} \simeq 0.08$, is smaller than the correlation length $\sigma = 0.2$.

In the limit of infinite repulsive interactions the system is ergodic [32] and $|\psi_0|$ is nearly constant in space, and thus independent of the disorder realization. It is worth noting that, in this limit, the ground state of the GPE is not macroscopically occupied and the gas of hardcore bosons behaves as a system of spinless fermions in the random potential V [75], according to the Tonks-Girardeau model.

1 Weak interactions

As it was pointed out in Ref. [57] where a pure harmonic potential was studied, for weak repulsive interactions, the spatial behavior of the ground state of the GPE can be understood through the one of the lowest-lying eigenstates of the noninteracting problem in Eq. (16), where H^{SP} is defined in Eq. (11). We will later show that these eigenstates can be approximated using the LL theory.

For a low nonlinear coefficient, $g(N-1) \lesssim 1$, the ground state ψ_0 of the GPE can be indeed expressed as a linear combination of the N_s eigenstates of H^{SP} (in Eq. (11)) whose energy does not exceed E^{th} . This energy threshold is defined as:

$$E^{\text{th}} := E_0^{\text{SP}} + \frac{g(N-1)}{2} \int_{-L/2}^{L/2} |\psi_0^{\text{SP}}(x)|^4 dx. \quad (24)$$

The number of SP states N_s contributing to the expression for ψ_0 thus must satisfy

$$N_s = n^{\text{SP}}(E^{\text{th}}), \quad (25)$$

where n^{SP} indicates the integrated density of SP states (IDoS) evaluated at E^{th} .

The ground state of the GPE can be then written as:

$$\psi_0(x) \approx \sum_{j=0}^{N_s-1} c_j \psi_j^{\text{SP}}(x), \quad (26)$$

where the coefficients $\{c_j\}$ must satisfy $\sum_{j=0}^{N_s-1} |c_j|^2 = 1$. While in the harmonic case the coefficients related to odd eigenfunctions vanish due to the parity symmetry of the potential, here, since the speckle potential lacks any spatial symmetry, the $\{c_j\}$ of the lowest-energy states can be all nonzero and can be evaluated as follows. By plugging Eq. (26) into the Gross-Pitaevskii equation (5) and multiplying both members on the left by the eigenstate ψ_m^{SP} of H^{SP} , the following relation among the coefficients $\{c_i\}$ is found:

$$c_m(E_m^{\text{SP}} - \mu) = g(N-1) \sum_{j,k,n=0}^{N_s-1} c_j^* c_k c_n \mathcal{I}_{mjkn}, \quad (27)$$

where the sum of the squared moduli of the coefficients is normalized to unity and

$$\mathcal{I}_{mjkn} := \int_{-L/2}^{-L/2} \psi_m^{\text{SP}*}(x) \psi_j^{\text{SP}*}(x) \psi_k^{\text{SP}}(x) \psi_n^{\text{SP}}(x) dx. \quad (28)$$

Reminding the definition of the chemical potential in Eq. (10), that equation can be rewritten as:

$$\begin{aligned} c_m \left(E_m^{\text{SP}} - \sum_{j=0}^{N_s-1} |c_j|^2 E_j^{\text{SP}} \right) &= \\ &= g(N-1) \sum_{i,j,k,n=0}^{N_s-1} (\delta_{im} - c_i^*) c_j^* c_k c_n \mathcal{I}_{ijkn}, \end{aligned} \quad (29)$$

where δ_{im} is the Kronecker's delta between the SP eigenstates ψ_i^{SP} and ψ_m^{SP} . By finding the equation (29) for each coefficient c_i with $i = 0, 1, \dots, N_s - 1$, one obtains a system of nonlinear coupled equations, whose solution is carried out by exploiting the approximations detailed in App. B.

Labeling as ψ_0^{lcs} the state approximated using the *linear combination of SP states* in Eq. (26), the total energy of the gas E_0^{lcs} can be evaluated in this framework by inserting the right-hand side of Eq. (26) into Eq. (9), thus obtaining:

$$\begin{aligned} E_0^{\text{lcs}} &:= \sum_{j=0}^{N_s-1} |c_j|^2 E_j^{\text{SP}} + \\ &+ \frac{g(N-1)}{2} \int_{-L/2}^{L/2} \left| \sum_{j=0}^{N_s-1} c_j \psi_j^{\text{SP}}(x) \right|^4 dx. \end{aligned} \quad (30)$$

By plugging the right-hand side of Eq. (26) into Eq. (10),

the chemical potential can be analogously expressed as:

$$\begin{aligned} \mu^{\text{lcs}} := & \sum_{j=0}^{N_s-1} |c_j|^2 E_j^{\text{SP}} + \\ & + g(N-1) \int_{-L/2}^{L/2} \left| \sum_{j=0}^{N_s-1} c_j \psi_j^{\text{SP}}(x) \right|^4 dx. \end{aligned} \quad (31)$$

The SP eigenstates, necessary for computing ψ_0^{lcs} , E_0^{lcs} and μ^{lcs} can also be efficiently computed by starting from the LL.

The correspondence between the position of the lowest minima of the effective potential and the localization centers of the lowest-lying SP states has been indeed illustrated in Ref. [63, 76]. In the former work, it is also proved that the domain Ω_i of the i -th lowest-lying SP state can be identified as the connected region where $V_{\text{LL}}(x) \leq E_i^{\text{SP,LL}}$, containing the i -th lowest minimum of V_{LL} . The energy $E_i^{\text{SP,LL}}$ of the lowest-lying SP states can be estimated using an empirical formula introduced in Ref. [63]:

$$E_i^{\text{SP,LL}} = \left(1 + \frac{d}{4}\right) V_{\text{LLmin},i}, \quad (32)$$

where $V_{\text{LLmin},i}$ now denotes the *absolute* minimum of the effective potential in the domain Ω_i . The SP wavefunction of the i -th excited state, whose support lies in Ω_i , can be expressed as

$$\psi_i^{\text{SP,LL}}(x) = \frac{u(x)}{\left(\int_{\Omega_i} |u(x)|^2 dx\right)^{1/2}}, \quad (33)$$

as pointed out in Ref. [63]. By plugging Eqs. (32) and (33) into (24), one can also find the energy threshold for the SP states within the LL approach:

$$E^{\text{th,LL}} := \left(1 + \frac{d}{4}\right) V_{\text{LLmin},0} + \frac{g(N-1)}{2} \frac{\mathcal{J}_4^{\text{SP}}}{(\mathcal{J}_2^{\text{SP}})^2}. \quad (34)$$

In Eq. (34), $\mathcal{J}_l^{\text{SP}}$ labels the integral:

$$\mathcal{J}_l^{\text{SP}} := \int_{\Omega_0} |u(x)|^l dx, \quad (35)$$

where $l = 2, 4$.

Coherently with the analysis carried out so far, the same quantities are also evaluated by using the LL. By taking advantage of Eq. (32), the total energy can be in

fact expressed as

$$\begin{aligned} E_0^{\text{lcs,LL}} := & \sum_{j=0}^{N_s^{\text{LL}}-1} \left(1 + \frac{d}{4}\right) V_{\text{LLmin},j} |c_j^{\text{LL}}|^2 + \\ & + \frac{g(N-1)}{2(\mathcal{J}_2^{\text{SP}})^2} \sum_{i,j,k,l=0}^{N_s^{\text{LL}}-1} c_i^{\text{LL}*} c_j^{\text{LL}*} c_k^{\text{LL}} c_l^{\text{LL}} \int_{\Omega_i \cap \Omega_j \cap \Omega_k \cap \Omega_l} |u(x)|^4 dx. \end{aligned} \quad (36)$$

Similarly to Eq. (31), the chemical potential in the LL approximation can be written as:

$$\begin{aligned} \mu^{\text{lcs,LL}} := & \sum_{j=0}^{N_s^{\text{LL}}-1} \left(1 + \frac{d}{4}\right) V_{\text{LLmin},j} |c_j^{\text{LL}}|^2 + \\ & + \frac{g(N-1)}{(\mathcal{J}_2^{\text{SP}})^2} \sum_{i,j,k,l=0}^{N_s^{\text{LL}}-1} c_i^{\text{LL}*} c_j^{\text{LL}*} c_k^{\text{LL}} c_l^{\text{LL}} \int_{\Omega_i \cap \Omega_j \cap \Omega_k \cap \Omega_l} |u(x)|^4 dx. \end{aligned} \quad (37)$$

In order to numerically test the validity of this approach, we consider an ultracold Bose gas in a speckle potential with the same values of parameters V_0 and σ as in Fig. 4, but a different disorder realization in a shorter 1D domain, represented in Fig. 5a. The ground state of the GPE is computed for $g(N-1) = 1$ and plotted in Fig. 5b by the dark-blue short-dashed lines respectively. For the former value of the nonlinear coefficient, the number of relevant SP eigenstates of H^{SP} contributing to the expansion (26) amounts to $N_s = 4$, value that is reckoned by using Eqs. (25) and (24). The four lowest-lying SP eigenstates, vanishing at the boundaries of the domain and computed by exact diagonalization of the SP Hamiltonian, are therefore plotted in Fig. 5b by the solid lines.

Furthermore, from Fig. 5, one can infer that the absolute maxima of the SP eigenstates occur at the lowest minima of the effective potential V_{LL} . In particular, the squared modulus of ψ_0^{SP} reaches its maximum at the absolute minimum of the effective potential V_{LL} , as pinpointed by the red arrow in Fig. 5a. The other SP states possess their absolute maxima at the local minima of V_{LL} indicated by the other arrows in the same figure. Unlike the other SP states in Fig. 5b, the excited state ψ_2^{SP} possesses a node, located at $x \approx 21$, in rough correspondence with a local maximum of V_{LL} .

For the situation in Fig. 5, we compute the coefficients $\{c_i\}$ from the solution of Eq. (29) with $m = 0, 1, \dots, N_s - 1$, involving the SP states and energies computed by two different methods: exact diagonalization of H^{SP} and LL (in Eqs. (32) and (33)). The moduli of the coefficients $\{c_i\}$ found with the former method are presented in the fourth column of Tab. I, the ones computed using the latter method and labeled as $\{|c_i^{\text{LL}}|\}$ are exposed in the fifth column. While using the exact diagonalization one obtains $N_s = 4$, the number of relevant SP eigenstates computed within the LL-based approach, by evaluating the IDoS at $E^{\text{th,LL}}$ in Eq. (34), amounts to $N_s^{\text{LL}} = 3$. The agreement between the two sets of values appears

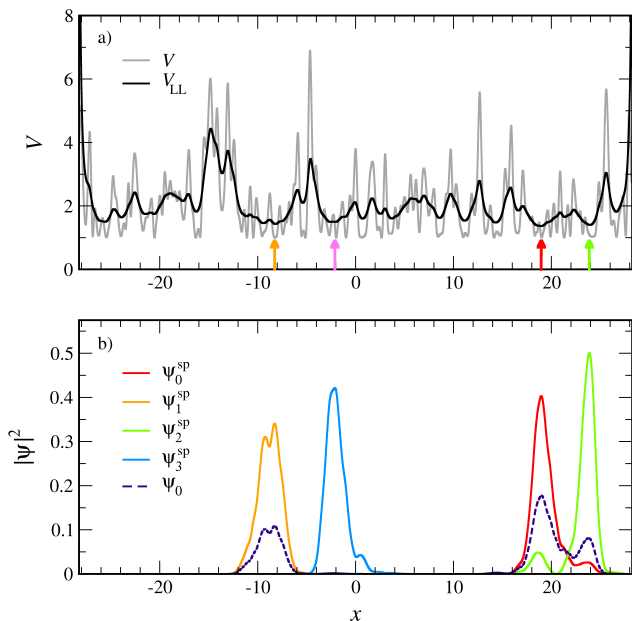


FIG. 5. Weakly repulsive interactions and SP states. Panel (a): original potential V and effective potential V_{LL} computed using the same values of V_0 , σ and numerical lattice spacing a as in Fig. 4, for a domain of length $L = 16,000a$. The arrows indicate the four lowest minima of V_{LL} where the lowest-lying SP states reach their absolute maxima. Panel (b): probability amplitudes associated to the four lowest-energy states $\{\psi_i^{SP}\}$ of the noninteracting Hamiltonian H^{SP} , satisfying the Dirichlet boundary conditions, plotted as solid lines. The aforementioned states are found by exact diagonalization of the SP Hamiltonian in Eq. (11). The dark-blue short-dashed line represents the ground state ψ_0 of the GPE, extracted for $g(N-1) = 1$.

to be quite satisfactory, in particular for the main two contributions, $|c_0|$ and $|c_1|$, where the deviation is about 6% on average. The significant discrepancy, in particular, occurring for the most excited states can be explained by the fact that the LL-based approximation in Eq. (33) is not able to describe as accurately the exponentially decaying behavior of the SP wavefunctions at the tails. Moreover, the SP wavefunctions do not occupy the lowest minima of V_{LL} in rigorous ascending order of energy, as also noticed in Ref. [63], and the SP energies computed by Eq. (32) appear to be overestimated by 9% on average, as it can be deduced from the second and the third columns of Tab. I. This amount turns out to be of the same order of the one found on average in the work just mentioned.

By using the two sets of coefficients in Tab. I, the ground state of the GPE in the approximation presented in Eq. (26) is evaluated using the SP eigenstates extracted by means of the two different approaches. The modulus squared of the wavefunction ψ_0^{lcs} computed with the coefficients $\{c_i\}$ is then represented in Fig. 6 as the blue long-dashed line, whereas the one obtained with the coefficients $\{c_i^{LL}\}$, indicated as $\psi_0^{lcs,LL}$, is por-

| i | E_i^{SP} | $E_i^{SP,LL}$ | $ c_i $ | $ c_i^{LL} $ |
|-----|------------|---------------|---------|--------------|
| 0 | 1.576 | 1.705 | 0.766 | 0.674 |
| 1 | 1.611 | 1.789 | 0.587 | 0.578 |
| 2 | 1.683 | 1.751 | 0.248 | 0.460 |
| 3 | 1.700 | 1.868 | 0.0823 | 0.0 |

TABLE I. Summary of the values of the energy and of the coefficients of the expansion (26) of ψ_0 in terms of the SP states. $\{E_i^{SP}\}$ and $\{c_i\}$ are computed by means of the eigenfunctions extracted by exact diagonalization of H^{SP} . $\{E_i^{SP,LL}\}$ and $\{c_i^{LL}\}$ are evaluated by using the SP eigenstates in the LL-based approximation in Eq. (33), with the eigen-energies in Eq. (32).

trayed as the black short-dashed line. In the same figure, both quantities are compared against the exact numerical $|\psi_0|^2$, which is plotted as the light-blue solid line. The very good agreement between the squared moduli of ψ_0 and ψ_0^{lcs} also ascertains the validity of the approach here used, based on the lowest-lying SP eigenstates. The superposition integral between the two last-mentioned wavefunctions, $\int \psi_0^*(x)\psi_0^{lcs}(x)dx$, yields 0.996. On the other hand, $\psi_0^{lcs,LL}$ is able to capture well the positions of the highest local maxima, but fails to account for the region where ψ_0^{SP} and ψ_2^{SP} overlap between each other. The overlap integral between ψ_0 and $\psi_0^{lcs,LL}$, $\int \psi_0^*(x)\psi_0^{lcs,LL}(x)dx$, amounts then to 0.901, a value which is farther from 1, thus reflecting the larger deviations between the states. Nevertheless, the landscape-based approximation becomes convenient for larger systems or for higher dimension, due to its much lower computational cost [63], compared to the diagonalization of the SP Hamiltonian, H^{SP} .

Furthermore, the total energy and the chemical potential associated to the ground state of the GPE in the SP-state expansion (in Eq. (26)) are computed by means of Eqs. (30) and (31) respectively. The values of the energy and the chemical potential thus found are compared with those obtained using the LL in Eqs. (36) and (37) in the second and the third columns of Tab. II, respectively.

In particular, the energy and the chemical potential obtained by using the exact ψ_0 (see Eqs. (9) and (10)) appear to be in excellent agreement with those found within the approximation based on the expansion in SP states extracted by exact diagonalization of H^{SP} , the deviation between the two estimates being of 3% at most. The discrepancies with the estimates based on the LL, $E_0^{lcs,LL}$ and $\mu^{lcs,LL}$ both amount to 10% instead and mirrors the overestimates noticed in the SP energies (in Tab. I).

Finally, it is worth noticing that the eigenstates of the GPE explainable as superpositions of SP states do not necessarily lie in the Lifshitz glass phase [46], since in that case the SP states do not spatially overlap (unlike the wavefunctions in Fig. 5) and belong to the Lifshitz tails of the IDoS.

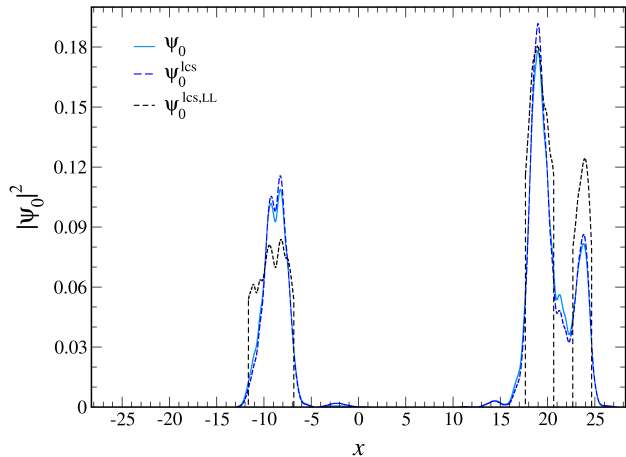


FIG. 6. Probability density associated to the ground state of the GPE for $g(N-1) = 1$ and the disorder configuration displayed in Fig. 5a, computed by means of three different methods. Wavefunction ψ_0 determined by time-evolution (light-blue solid line). $|\psi_0^{\text{ics}}|^2$ (dark-blue long-dashed line), referring to the approximation in Eq. (26), based on the SP eigenstates computed by exact diagonalization. $|\psi_0^{\text{ics,LL}}|^2$ (black short-dashed line), found in the approximation in Eq. (26), based on the SP eigenfunctions estimated using the LL in Eq. (33).

| Exact solution | SP-mode decomposition | |
|----------------|-----------------------|-----------------------|
| E_0 | E_0^{ics} | $E_0^{\text{ics,LL}}$ |
| 1.643 | 1.644 | 1.801 |
| μ | μ^{ics} | $\mu^{\text{ics,LL}}$ |
| 1.689 | 1.693 | 1.859 |

TABLE II. Comparison between the values of the energy and the chemical potential of the ground state of the GPE for $g(N-1) = 1$ in Fig. 6, obtained by three different procedures. First column: quantities computed by means of the Crank-Nicolson time-evolution algorithm. Second column: energy and chemical potential evaluated by using Eqs. (30) and (31) respectively. Third column: same quantities estimated by making use of Eqs. (36) and (37) respectively.

We have seen that, for weak repulsive interactions, the delocalization effect can be understood by introducing a perturbative approximation based on lowest-lying SP states, that can indeed apply for random potentials endowed with any spatial distribution and correlation profile. Besides, the LL, able to predict the location of each SP state, allows to quite accurately estimate the ground state of the GPE, as well as its energy and chemical potential, with a reduced computational cost. The evaluation of the SP ground state by exact diagonalization of H^{SP} has further allowed us to prove the consistence with the stationary state computed by the time-evolution algorithm for vanishing interactions. In the following sub-

section we will focus on the shape of the wavefunction ψ_0 for intermediate and strong repulsive interactions.

2 Intermediate and strong interactions

As proved in Ref. [29], when $\xi \gtrsim \sigma$, the length of the spatial modulations of the particle density can be only larger than the correlation length of the random potential V_{R} . The wavefunction of the ground state ψ_0 is then sensitive to the modulations of a potential V_{s} which is smoother than the original one, V . The former potential reads [29]:

$$V_{\text{s}}(x) = \int_{-L/2}^{L/2} G(x') V_{\text{R}}(x-x') dx', \quad (38)$$

where

$$G(x) = \frac{1}{\sqrt{2}\xi'} e^{-\frac{\sqrt{2}|x|}{\xi'}} \quad (39)$$

is the Green's function related to the disorder-free problem $(-\frac{\xi'^2}{2}\nabla^2 + 1)G(x) = \delta(x)$, in which $\xi' := \xi\sqrt{\frac{\mu}{\mu-1}}$. The macroscopical wave-function in this approximation, where the smoothed potential is treated as a perturbation with respect to the homogeneous case, ψ_0^{s} is given by [29]:

$$\psi_0^{\text{s}}(x) = \sqrt{\frac{\mu-1}{g(N-1)}} \left(1 - \frac{1}{2(\mu-1)} V_{\text{s}}(x) \right). \quad (40)$$

In addition, the validity of Eq. (40) is guaranteed as long as $\xi \ll L$ and $V_{\text{s}}(x) \ll \mu - 1$.

Within the smoothing regime thus defined, another approximation scheme, based on the effective potential $V_{\text{LL}}(x)$ and much less computationally expensive, is introduced:

$$|\psi_0^{\text{TF,LL}}(x)| = \begin{cases} \sqrt{\frac{\mu - V_{\text{LL}}(x)}{g(N-1)}} & \mu \geq V_{\text{LL}}(x) \\ 0 & \mu < V_{\text{LL}}(x) \end{cases}. \quad (41)$$

This scheme holds as long as $\sigma < \xi < \sigma_{\text{LL}}$, where σ_{LL} is the correlation length of the effective potential.

The approximations in Eqs. (40) and (41) cease to be valid also for $\xi > \sigma$, whereas the Thomas-Fermi approximation becomes very accurate for $\xi \ll \sigma$. Within this limit, the kinetic energy of the gas becomes negligible and the modulations of the original potential govern the spatial behaviour of the wavefunction ψ_0 , as shown at the beginning of this Section.

By considering the same disorder configuration as in Fig. 4, the result of the estimate of ψ_0 based on Eq. (41) is shown in Fig. 7, where it is compared to the usual Thomas-Fermi approximation in Eq. (23) and to the

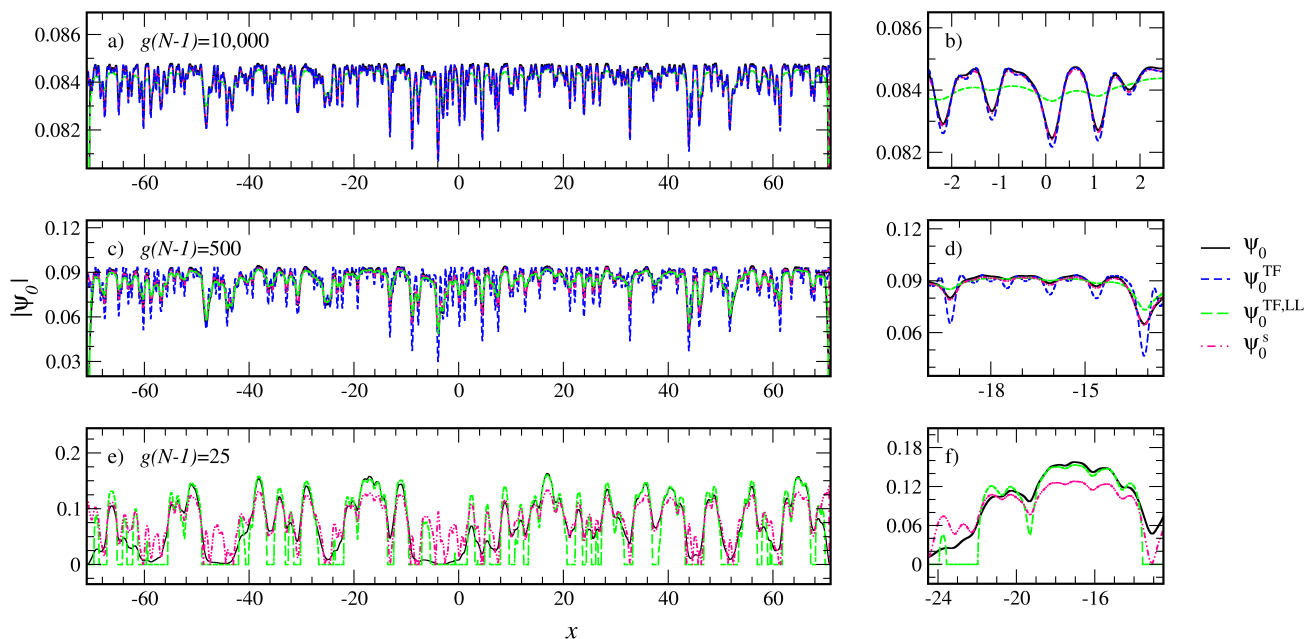


FIG. 7. Intermediate and strongly repulsive interactions. Panel (a): ground state of the GPE with the potential shown in Fig. 4a and for a nonlinear coefficient $g(N-1) = 10^4$. Wavefunction ψ_0 computed by time evolution (black solid line), by the Thomas-Fermi approximation ψ_0^{TF} (blue short-dashed line) in Eq. (23), by the landscape-based approximation $\psi_0^{\text{TF,LL}}$ (green long-dashed line) and by the perturbative method in Eq. (40) ψ_0^s (magenta doubly dotted-dashed line). Panel (b): the same quantities as in Panel (a), restricted to the interval $[-3, 3]$. Panel (c): the same quantities as in Panel (a), but related to the ground state of the GPE for $g(N-1) = 500$. Panel (d): the same quantities as in Panel (c), restricted to the interval $[-20, -12.5]$. Panel (e): the same quantities as in Panel (a), but related to the ground state of the GPE for $g(N-1) = 25$. Unlike in Panel (a), ψ_0^{TF} is here omitted, since the conditions of the Thomas-Fermi approximation are by far not satisfied. Panel (f): the same quantities as in Panel (e), restricted to the interval $[-25, -12.5]$.

smoothing approximation in Eq. (40) in Figs. 7a-d, and only with the latter scheme in Figs. 7e-f. In Figs. 7a-b, we show that, for strong interactions (as $g(N-1) = 10,000$), when also both the conditions $\xi < \sigma$ and $V_0 \ll \mu$ are fulfilled, the Thomas-Fermi approximation proves to be an excellent approximation, since the superposition integral with ψ_0 reaches 0.9997. Concomitantly, also the smoothed wavefunction ψ_0^s overlaps excellently with the exact numerical ground state, plotted by the black solid line, since $G(x) \approx \delta(x)$. The overlap integrals between ψ_0 and ψ_0^s and ψ_0^{TF} amount in fact both to 0.9997. Unlike ψ_0^{TF} , $\psi_0^{\text{TF,LL}}$ here appears to be far from the steady state ψ_0 of the Gross-Pitaevskii equation, whose behavior is ruled by the original potential V rather than the effective one, V_{LL} .

Figs. 7c-d represent the case in which $g(N-1) = 500$, where the healing length satisfies $\xi \gtrsim \sigma$ while the chemical potential $\mu \gg V_0$. Under these conditions, the Thomas-Fermi approach becomes inadequate, whereas $\psi_0^{\text{TF,LL}}$ approaches satisfactorily the wavefunction ψ_0 , with an overlap integral with ψ_0 which amounts to 0.9994. At the same time, ψ_0^s still represents a reliable approximation, since the superposition integral with ψ_0 yields 0.9983. Figs. 7e-f refer to the case in which $g(N-1) = 25$, characterized by a $\mu \sim V_0$ and still by

$\xi > \sigma$. Here, the perturbative approach introduced with the smoothing approximation ceases to be reliable, as well as -to a slightly lesser extent - the ansatz in Eq. (41).

To summarize, while for strong repulsive interactions, such that $\xi \ll \sigma$, we have recovered that the stationary state follows the Thomas-Fermi approximation [29], an analogous scheme based on the effective potential provides an efficient way to compute ψ_0 for $\xi \gtrsim \sigma$. However, this approach ceases to hold for $\xi \gg \sigma$, as the Bose gas gets fragmented. It is worthwhile to remark that the delocalizing effect on ψ_0 in the presence of increasingly strong repulsive interactions also qualitatively agrees with a previous result [77] obtained in the context of the (many-particle) Lieb-Liniger model with scatterers following the Poisson distribution and Dirichlet boundary conditions on ψ_0 .

B Exploring the mean disorder strength

To assess the effect of disorder on the spatial behavior of ψ_0 , we computed the latter quantity for different values of the parameter V_0 of the random potential, keeping the correlation length constant and equal to the one set in Ref. [4]. We begin considering the case of a repul-

sively interacting gas, using the same parameters as in Fig. 4, except for V_0 and $g(N-1) = 152$. In Fig. 8a, we plot the effective potentials V_{LL} with solid lines for three different values of V_0 , whereas in Fig. 8c we show the corresponding moduli of the wavefunctions ψ_0 . For the sake of readability, the total potentials V are only plotted in Fig. 8b with short-dashed lines, using the same colors of the corresponding effective potentials. As it can be noticed from Fig. 8, the modulus of the wavefunction at the maxima of the effective potential V_{LL} gets lower as V_0 is increased from $V_0 = 0.1V_0^{e,r}$ to $V_0 = 30V_0^{e,r}$. This reflects the fact that the energy E_0 becomes progressively smaller than V_0 as the latter quantity is raised. As a result, the condensate gets more tightly trapped by the potential and ultimately multi-fragmented [33, 46], i. e. roughly describable as a superposition of localized states.

As this confining effect becomes more pronounced, the effective potential V_{LL} gets closer to the original potential, as it can be deduced by Fig. 8b. This effect can be explained by making use of the correlation energy $E_\sigma := \frac{1}{2\sigma^2}$ [12], which represents the zero-point energy for a particle confined in a spatial region of size equal to the correlation length σ . As V_0 is increased, a *crossover* takes place from the quantum regime, characterized by the competition between quantum interference and tunnelling (where $V_0/E_\sigma < 1$), to the semiclassical one, dominated by the localization due to the barriers of potential, such that hopping is inhibited and $V_0/E_\sigma > 1$. Furthermore, in the region of the parameter space explored, the effective potential still allows to well predict the position of the maxima of the ground state ψ_0 , since $\xi \gtrsim \sigma$, as seen in Subsec IV A 2.

As noticed in this analysis, for very strong disorder, the ground state ψ_0 of the Gross-Pitaevskii equation tends to be a superposition of localized SP states which do not exhibit any overlap between each other, as opposed to those shown in Fig. 5b, and belong to the Lifshitz tails of the SP spectrum. The Bose gas thus becomes a Lifshitz glass, where the gas splits into mini-condensates that occupy the lowest-lying SP states, satisfying the condition $E_i^{sp} \leq \mu$. According to the landscape theory, these states are expected to occur at the deepest wells of the effective potential V_{LL} , whose occupation number increases as the SP localization length gets larger. The number of particles N_i^{sp} associated to each one-particle wavefunction ψ_i^{sp} can be thus evaluated using the following relation [46]:

$$N_i^{sp} = \begin{cases} \frac{\mu - E_i^{sp}}{U_i} & \text{for } \mu < E_i^{sp} \\ 0 & \text{for } \mu \geq E_i^{sp} \end{cases}, \quad (42)$$

where $U_i := g \int_{-L/2}^{L/2} dx |\psi_i^{sp}(x)|^4$ and N_s is the number of SP states. The numbers of particles satisfy

$$\sum_{i=0}^{N_s-1} N_i^{sp} = N, \quad (43)$$

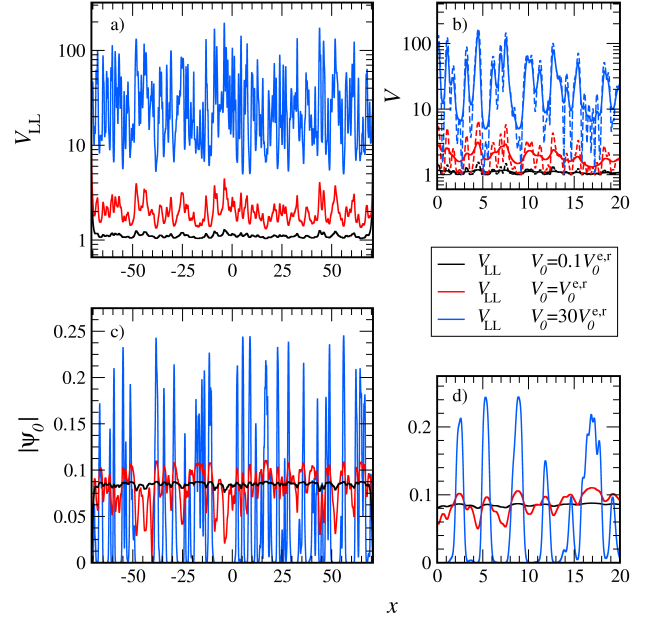


FIG. 8. Repulsively-interacting Bose gases with $g(N-1) = 152$ in speckle potentials with different values of V_0 and correlation length $\sigma = 0.2$ in a domain of length $L = 40,000a$, where $a = 0.0035$. Panel (a): effective potentials V_{LL} (solid lines) for different mean values V_0 of the speckle potential: $V_0 = 0.1V_0^{e,r}$ (black lines), $V_0 = V_0^{e,r}$ (red lines), $V_0 = 30V_0^{e,r}$ (blue lines). Panel (b): the same quantities as in Panel (a), restricted to the spatial interval $[0, 20]$. Original potentials V (short-dashed lines with the same colors of the corresponding effective potentials). Panel (c): ground states of the 1D GPE in Eq. (5) for the three mean values V_0 last mentioned (solid lines). Panel (d): the same quantities as in Panel (c), but plotted in the same spatial interval as in Panel (b).

and the chemical potential associated to the many-particle state can be written as

$$\mu = \frac{N + \sum_{i=0}^{N_s-1} \frac{E_i^{sp}}{U_i}}{\sum_{i=0}^{N_s-1} U_i^{-1}}. \quad (44)$$

Reminding the relation (10), the energy of the ground state ψ_0 of the GPE can be now expressed as:

$$E_0 = \frac{1}{2N} \sum_{i=0}^{N_s-1} \frac{(\mu^2 - E_i^{sp 2})}{U_i}. \quad (45)$$

In order to assess how the LL is able to predict ψ_0 , its energy and chemical potential, we approximate each SP state using Eq. (33) and estimate its energy by exploiting Eq. (32).

To this purpose, we dwell upon a realization of the random potential with an increased mean value $V_0 = 73$ (compared the ones displayed in Fig. (8)) and a smaller correlation length $\sigma = 8.1 \cdot 10^{-4}$ and we consider a Bose

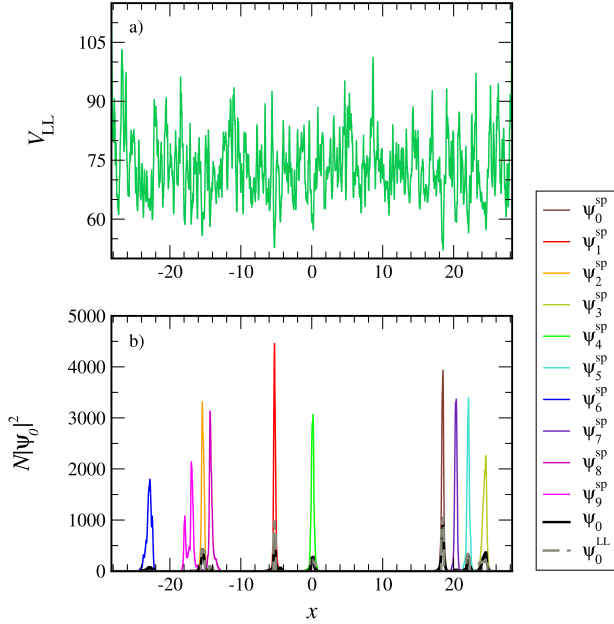


FIG. 9. Lifshitz glass phase. A repulsively interacting gas with $g(N-1) = 12.6$ and $N = 1,403$ atoms of ^{87}Rb in a 1D speckle potential with typical amplitude $V_0 = 73$ and correlation length $\sigma = 8.1 \cdot 10^{-4}$ in a domain of length $L = 16,000a$ with $a = 0.0035$. Panel (a): effective potential V_{LL} (green solid line). Panel (b): the particle densities $\{N|\psi_i^{\text{SP}}|^2\}$ associated to the 10 lowest-lying SP eigenstates of H^{SP} (solid lines). Particle density $N|\psi_0|^2$ related to the ground state of the GPE computed by time-evolution (thick black solid line), and the one evaluated by approximating the SP eigenstates using Eq. (33), denoted as $N|\psi_0^{\text{LL}}|^2$ (thick gray long-dashed-dotted line).

gas of $N = 1,403$ particles. Owing to the smallness of the correlation length ($\sigma \ll \xi$), the spacing between the single-particle energy levels is still lower than 1, thus justifying again the goodness of the factorization of $\psi_0(\mathbf{r})$ in Eq. (3), despite the high value of V_0 . The ground state computed by time-evolution, portrayed as the thick black curve in Fig. 9b, is nonvanishing along the support of the first $N_s = 9$ lowest-lying eigenstates of the single-particle problem (11), computed by exact diagonalization and represented by the solid lines (from brown to violet).

Compared to the case examined in Sec. IV A 1, N_s here is no longer predicted by Eq. (24), which, in the case of Fig. 9, would lead to an overestimate of that number, thus yielding an upper energy limit for the SP states $E^{\text{th}} = 73.2$ since the interaction is not small enough. Besides, the exact diagonalization allows to determine values of the energy and the chemical potential (in Eqs. (45) and (44) respectively) which are in excellent agreement with those associated to the exact numerical ψ_0 , as witnessed by the values exposed in the columns 1-2 in Tab. IIIb. This result also confirms that Eqs. (42)-(44), together with the normalization condition in Eq. (43),

allow to well set the number of SP states which contribute to the many-particle state ψ_0 . Since the exact lowest-lying SP states do not occupy the lowest minima of the effective potential in rigorous ascending order of energy, the LL-based predictions concern a slightly different set of SP eigenstates, as shown in the fifth column of Tab. IIIa. Hence, both the total energy and the chemical potential in the third column of Tab. IIIb appear to differ from the estimates above mentioned, by about 8% and 10% respectively.

Starting from Eq. (42), the occupation numbers of the SP states evaluated from the exact diagonalization are denoted as $\{N_i^{\text{SP}}\}$. The same quantities computed by using the states estimated by the LL in Eq. (33), are indicated as $\{N_i^{\text{SP,LL}}\}$ instead. Both these sets of numbers are compared in Tab. III to those extracted by integrating the eigenstate of the GPE along the support of each SP wavefunction and labelled as $\{N_i^{\text{SP,GPE}}\}$. The boundaries of each support are numerically estimated by identifying the points where $\psi_i^{\text{SP}}(x)$ decreases to values lower than 0.05 and the integrations are accurately performed using the Cavalieri-Simpson's 3/8 rule. As it can be inferred, the three estimates agree quite well for the six lowest-energy states, for which the discrepancy with respect to $\{N_i^{\text{SP,GPE}}\}$ amounts to the 6% on average for the $\{N_i^{\text{SP}}\}$, and to 14% for the $\{N_i^{\text{SP,LL}}\}$. The evaluation of $\{N_i^{\text{SP,LL}}\}$ allows then to obtain the ground state ψ_0^{LL} , represented as the thick gray long-dashed-dotted curve in Fig. 9b. As one can also infer from Fig. 9b, the LL is able to capture six out of the nine main peaks of the numerical ground state ψ_0 , and the overlap integral $\int_{-L/2}^{L/2} \psi_0^*(x)\psi_0^{\text{LL}}(x) dx$ with that quantity amounts to 0.849. This result suggests a quite good accuracy of the landscape-based scheme in the Lifshitz glass phase.

A numerical proof of the belonging of the aforementioned SP states to the Lifshitz tails is given by the behavior of the IDoS. The latter quantity is defined as

$$n^{\text{SP}}(E^{\text{SP}}) = \int_{E_{\text{min}}^{\text{SP}}}^{E^{\text{SP}}} \rho^{\text{SP}}(E') dE', \quad (46)$$

where ρ represents the density of states, which is normalized to the total number of particles in the Bose gas: $\int_{E_{\text{min}}^{\text{SP}}}^{E_{\text{max}}^{\text{SP}}} \rho^{\text{SP}}(E') dE' = N$. In 1D systems, the IDoS is characterized by exponentially decaying edges, known as the Lifshitz tails [78, 79]:

$$n^{\text{SP}}(E^{\text{SP}}) \approx C_1 e^{-\frac{C_2}{\sqrt{E^{\text{SP}} - C_3}}}, \quad (47)$$

where C_j with $j = 1, 2, 3$ are dimensional constants, of which C_3 should approach the minimum value of the random potential [46]. Considering the same configuration of the disordered potential as in Fig. 9a, we compute both the density of states ρ^{SP} , represented in Fig. 10a as the green solid line, and the integrated one n^{SP} , plotted in

| i | E_i^{SP} | $N_i^{\text{sp,GPE}}$ | N_i^{sp} | $N_i^{\text{sp,LL}}$ |
|-----|-------------------|-----------------------|-------------------|----------------------|
| 0 | 61.328 | 362 | 336 | 345 |
| 1 | 63.481 | 233 | 196 | 289 |
| 2 | 64.236 | 204 | 201 | 217 |
| 3 | 64.482 | 260 | 265 | 214 |
| 4 | 65.079 | 134 | 146 | 148 |
| 5 | 65.140 | 128 | 138 | 143 |
| 6 | 66.323 | 63 | 97 | 0 |
| 7 | 66.709 | 11 | 20 | 0 |
| 8 | 67.655 | 3 | 0 | 43 |
| 9 | 67.770 | 0 | 0 | 1 |

(a)

| E_0 | E_0^{GPE} | E_0^{LL} |
|--------|--------------------|-------------------|
| 65.433 | 65.444 | 70.989 |
| μ | μ^{GPE} | μ^{LL} |
| 67.028 | 66.897 | 73.388 |

(b)

TABLE III. Lifshitz glass phase. Table (a): summary of the ten lowest-lying SP energy values $\{E_i^{\text{SP}}\}$ and the numbers of particles in each SP state (estimated by using three different methods), related to the system in Fig. 8. From column 1 to 2: SP state labels and SP state eigen-energies, computed by exact diagonalization. From column 3 to column 5: the numbers of bosons in each SP state computed by integration around the peaks of the ground state of the GPE ($N_i^{\text{sp,GPE}}$), the ones evaluated by using Eq. (42) with SP states by exact diagonalization (N_i^{sp}), the ones estimated by means of Eq. (42) with SP states by LL ($N_i^{\text{sp,LL}}$). Table (b): the total energy of the Bose gas and its chemical potential, estimated starting from the data found by the three methods above mentioned.

Fig. 10b as the black solid line, displayed also in the inset. From a nonlinear regression, with correlation coefficient 0.872, we find $C_1 = 7.69 \cdot 10^4$, $C_2 = 99.8$ and $C_3 = -4.59$. The values of the parameters $\{C_i\}$, with $i = 1, 2, 3$, are expected to vary according to the probability distribution and correlation of the random potential [80], and also to the disorder realization. While the agreement between the fitting curve and the numerical data appears to be rather good, as highlighted in Fig. 10b, C_3 is of the same order but still somewhat far from the prediction $\overline{C_3} = \min_{x \in [-L/2, L/2]} V(x) = 1.0$ valid for the average over the disorder configurations [46], signaling that the system is still not self-averaging.

The results of this subsection show that, for increasing disorder mean amplitude and fixed repulsive interaction, the delocalized ground state becomes increasingly fragmented. This ultimately gives rise to the appearance of the Lifshitz glass phase, where the Bose gas splits into mini-condensates localized on SP states which do not spatially overlap and belong to the Lifshitz tails of the SP IDoS. Here the ground state of the GPE can be effec-

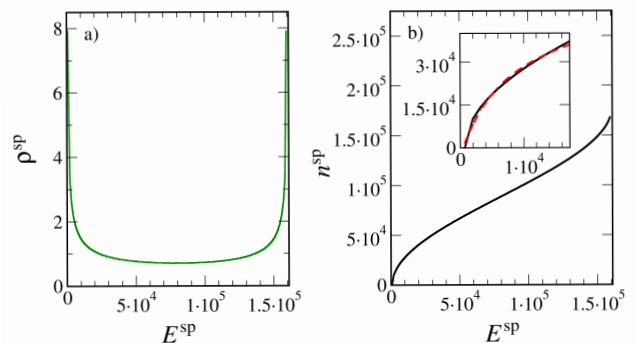


FIG. 10. Lifshitz tails of the IDoS. Panel (a): the density of SP states ρ^{SP} (green solid line) as a function of the energy. Panel (b): the integrated density of states n^{SP} (black solid line) as a function of the SP energy. In the inset, the two last-mentioned quantities are plotted against the fitting curve (orange long-dashed line) in a smaller interval of energies. This curve reflects Lifshitz's prediction [78] on the tails of n^{SP} in 1D disordered systems, exposed in Eq. (47).

tively approximated by exploiting the estimates of the SP states obtained by using the LL. We also point out that finiteness of the number of wells occupied by the wavefunction ψ_0 under those conditions was also proved by Seiringer *et al.* [77] within the Lieb-Liniger model with randomly distributed potential barriers.

V CONCLUSIONS AND PERSPECTIVES

We have presented here the numerical computation of the ground state of the quasi-1D Gross-Pitaevskii equation with Gaussian-correlated speckle potentials for a broad range of disorder parameters and nonlinear couplings. The spatial behavior of the state ψ_0 has been analyzed in relation with the original potential V and the effective potential V_{LL} , which is given by the reciprocal of the LL function. New approaches, based on the LL have been introduced for ψ_0 in the different phases (shaded areas in the quantum-state diagram in Fig. 11), in the regions of the interaction-disorder plane pinpointed by the violet signs.

For attractive interactions, which lead to the exponential localization of the atoms, we have unveiled an approximate relation between the disorder-averaged localization length and the nonlinear coefficient.

Unlike in the repulsive case, the LL is not able to explain the spatial behavior of ψ_0 for $g < 0$ and a possible alternative would be to test the landscape function associated to a nonlinear differential equation. In addition, the goodness of the functional relation for the localization length in Eq. (19) can be also tested in 2D systems, where the extent of ψ_0 might be reckoned by introducing a properly modified definition of the Agmon's distance [58, 63, 81].

For weak repulsive interactions $g(N-1) \lesssim 1$, we

have proved that the ground state of the Gross-Pitaevskii equation is well approximated by an expansion in terms of a finite number of single-particle states $\{\psi_i^{\text{SP}}\}$. For intermediate repulsive interactions, when $\sigma < \xi < \sigma_{LL}$, we have assessed an approximation of ψ_0 , based on a Thomas-Fermi-like ansatz using the effective potential, showing that, in this regime, ψ_0 follows the modulations of the effective potential rather than those of the original one. Nevertheless, when this approximation breaks down, the expansion in SP states is not convenient anymore, since $g(N-1)$ can be much larger than 1 and a suitable theoretical approach is still missing.

We have also reckoned the occupation number of each SP state by taking advantage of the LL, when the Bose gas takes the form of a Lifshitz glass.

The approaches here introduced have managed to increase our knowledge of the solutions of the time-independent GPE. These schemes can also be applied for random potentials endowed with any spatial distribution, on the condition that the correlation profile has a finite range. For long-range correlations in the disorder, the above methods might be not suitable since they can hinder localization, leading to the occurrence of mobility edges even in the noninteracting case [82] and they inhibit the fragmentation occurring for defocusing GPEs [32].

Furthermore, the results presented in this work can help to structure systems with higher-dimensional random potentials, whose phase diagram is more partially known [47, 48, 83] and where the features of the wavefunctions have been estimated only for superpositions of Gaussian and harmonic potentials [32], between the latter and the speckle ones [29], as well as for Bernoulli potentials [84]. For instance, the application of the localization-landscape theory to the density of states [64] may be helpful in accounting for the numerical phase boundary between the normal and the superfluid phase [48, 83] which occurs in 2D random potentials.

Moreover, it would be of interest to understand how our results would be modified in the presence of beyond-mean-field effects [85], like finite-range interactions, in low-dimensional disordered systems [86].

VI ACKNOWLEDGMENTS

We gratefully acknowledge V. Josse, A. Aspect, S. Mayboroda, D. N. Arnold, D. Delande, T. Bourdel, J.-P. Banon, A. Seye, P. Pelletier and L. Chen for fruitful discussions. This work was supported by grants from the Simons Foundation (Grants No. 601944, MF; No. 601950, YM) within the framework of the project *Localization of Waves*. For the numerical simulations, access was granted to the computational resources of the Mésocentre de Moulon in Gif-sur-Yvette (France).

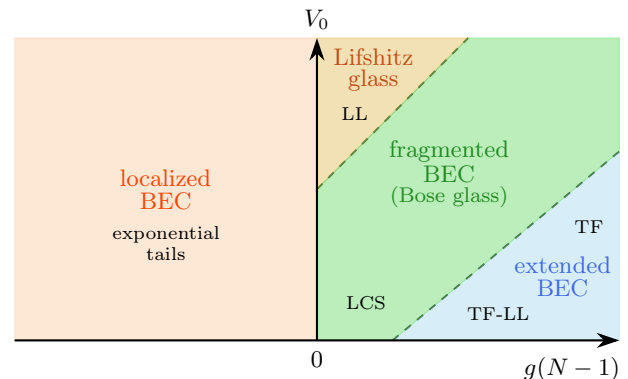


FIG. 11. Schematic quantum-state diagram in the interaction-disorder plane in which the abbreviations denote the approximations used for ψ_0 throughout the paper: the linear combination of states (LCS) for weakly repulsive interactions, the LL-based approximation in the Lifshitz glass phase, the Thomas-Fermi-like approximation (TF-LL) for intermediate repulsive interactions ($\sigma_{LL} < \xi < \sigma$), and the Thomas-Fermi approach for strongly repulsive interactions ($\xi \gg \sigma$). The dashed lines refer to the crossovers between each phase.

APPENDIX A: EVALUATION OF THE CHEMICAL POTENTIAL FOR ATTRACTIVE INTERACTIONS

In this subsection we describe the procedure and the analytical approximations that are at the basis of Eq. (18) for the chemical potential. Considering a large and self-averaging system with $L \gg \lambda_L, \lambda_R$ and taking $\lambda_R = \lambda_L =: \lambda$, the modulus of the wave-function becomes:

$$|\psi_0(x)| \approx c_a \begin{cases} e^{\frac{(x-x_0)}{\lambda}} & -\frac{L}{2} \leq x < x_0 \\ 1 & x = x_0 \\ e^{-\frac{(x-x_0)}{\lambda}} & x_0 < x \leq \frac{L}{2} \end{cases}, \quad (\text{A.1})$$

where the normalization constant now reads

$$c_a := \frac{1}{\sqrt{\lambda \left[1 - e^{-\frac{L}{\lambda}} \cosh\left(\frac{2x_0}{\lambda}\right) \right]}}. \quad (\text{A.2})$$

We first insert the right-hand side of Eq. (A.1) into the right-hand side of Eq. (10) and perform the integrations related to the kinetic and the interaction terms. By defining $f_a(\lambda) := \lambda^{-1} c_a^{-2}(\lambda)$ and following these steps, we

find:

$$\begin{aligned} \mu = & \frac{1}{2\lambda^2} + 1 + \frac{1}{\lambda f_a(\lambda)} \left[\int_{-L/2}^{x_0} V_R(x) e^{\frac{2(x-x_0)}{\lambda}} dx + \right. \\ & \left. + \int_{x_0}^{L/2} V_R(x) e^{-\frac{2(x-x_0)}{\lambda}} dx \right] + \\ & + \frac{g(N-1)}{2\lambda} \frac{f_a(\lambda/2)}{f_a^2(\lambda)}. \end{aligned} \quad (\text{A.3})$$

Since $L \gg \lambda$, the factors f_a in Eq. (A.3) converge to 1, whereas each of the two integrals involving the random potential V_R can be approximated as $\lambda V_0/2$. By carrying out these substitutions, one finally obtains the right-hand side of Eq. (18), which binds the chemical potential to the

parameters of the GPE.

APPENDIX B: EVALUATION OF THE COEFFICIENTS OF THE EXPANSION FOR WEAK REPULSIVE INTERACTIONS

In this subsection we outline the analytical approximation followed to efficiently solve the system of nonlinear coupled equations (29) for the coefficients $\{c_i\}$. Among the N_s^4 overlap integrals involved in Eq. (29), the most important contributions are those of the N_s^3 integrals containing at least two identical wavefunctions. Moreover, assuming real-valued eigenfunctions, the number of relevant integrals reduces to $N_s + \frac{3}{2}N_s! \left(\frac{1}{(N_s-2)!} + \frac{1}{(N_s-3)!} \right)$ and the summations on the right-hand side of Eq. (29) become:

$$\begin{aligned} \sum_{i,j,k,n=0}^{N_s-1} (\delta_{im} - c_i^*) c_j^* c_k c_n \mathcal{I}_{ijkn} \approx & \sum_{i=0}^{N_s-1} (c_i^4 - \delta_{im}) c_m^3 \mathcal{I}_{iiii} + \sum_{i \neq j}^{N_s-1} (4c_i^3 c_j - c_i^2 \delta_{jm} - 3c_j c_m^2 \delta_{im}) \mathcal{I}_{iiij} + \\ & + 3 \sum_{i>j}^{N_s-1} (2c_i^2 c_j^2 - c_i^2 c_m \delta_{jm}) \mathcal{I}_{iiij} + 6 \sum_{\substack{i>j \\ j>k}}^{N_s-1} (2c_i^2 c_j c_k - \delta_{im}) \mathcal{I}_{iijk} + \\ & + 3 \sum_{\substack{i>j \\ j>k}}^{N_s-1} (4c_i c_j^2 c_k - c_j^2 c_k \delta_{im}) \mathcal{I}_{ijjk} + 3 \sum_{\substack{i>j \\ j>k}}^{N_s-1} (4c_i c_j c_k^2 - c_j c_k^2 \delta_{im}) \mathcal{I}_{ijkk}. \end{aligned} \quad (\text{A.4})$$

Under the same assumptions, the following contributions to the left-hand side of Eq. (A.4) are therefore neglected:

$$6 \sum_{\substack{i>j \\ j>k \\ k>l}}^{N_s-1} (4c_i c_j c_k c_l - c_j c_k c_l \delta_{im}) \mathcal{I}_{ijkl}, \quad (\text{A.5})$$

since they involve integrals over four different one-

particle eigenfunctions. As Eqs. (A.4) for $m = 0, 1, \dots, N_s$ are polynomial relations up to the fourth order in the coefficients, manifold solutions are possible, all occurring in couples with opposite signs and satisfying the normalization condition, except for the trivial (and unphysical) one, characterized by all vanishing $\{c_i\}$. The most appropriate solution for the ground state of the GPE (5) is then identified as the one which minimizes the total energy.

-
- [1] M. Lewenstein, A. Sanpera, V. Ahufinger, B. Damski, A. Sen De, and U. Sen, Ultracold atomic gases in optical lattices: mimicking condensed matter physics and beyond, *Adv. Phys.* **56**, 243 (2007).
 - [2] M. H. Anderson, J. R. Ensher, M. R. Matthews, C. E. Wieman, and E. A. Cornell, Observation of Bose-Einstein condensation in a dilute atomic vapor, *Science* **269**, 198 (1995).
 - [3] F. Dalfovo, S. Giorgini, L. Pitaevskii, and S. Stringari, Theory of Bose-Einstein condensation in trapped gases, *Rev. Mod. Phys.* **71**, 463 (1999).
 - [4] J. Billy, V. Josse, Z. Zuo, A. Bernard, B. Hambrecht, P. Lugan, D. Clément, L. Sanchez-Palencia,

- P. Bouyer, and A. Aspect, Direct observation of Anderson localization of matter-waves in a controlled disorder, *Nature* **453**, 891 (2008).
- [5] G. Roati, C. D'Errico, L. Fallani, M. Fattori, C. Fort, M. Zaccanti, G. Modugno, M. Modugno, and M. Inguscio, Anderson localization of a non-interacting Bose-Einstein condensate, *Nature* **453**, 895 (2008).
- [6] F. Jendrzejewski, A. Bernard, K. Müller, P. Cheinet, V. Josse, M. Piraud, L. Pezzé, L. Sanchez-Palencia, A. Aspect, and P. Bouyer, Three-dimensional localization of ultracold atoms in an optical disordered potential, *Nat. Phys.* **8**, 398 (2012).
- [7] V. V. Volchkov, M. Pasek, V. Denechaud, M. Mukhtar,

- A. Aspect, D. Delande, and V. Josse, Measurement of spectral functions of ultracold atoms in disordered potentials, *Phys. Rev. Lett.* **120**, 060404 (2018).
- [8] P. W. Anderson, Absence of diffusion in certain random lattices, *Phys. Rev.* **109**, 1492 (1958).
- [9] F. Evers and A. D. Mirlin, Anderson transitions, *Rev. Mod. Phys.* **80**, 1355 (2008).
- [10] E. Abrahams, *50 Years of Anderson Localization* (World Scientific, 2010).
- [11] S. S. Kondov, W. R. McGehee, W. Xu, and B. DeMarco, Disorder-induced localization in a strongly correlated atomic hubbard gas, *Phys. Rev. Lett.* **114**, 083002 (2015).
- [12] B. Shapiro, Cold atoms in the presence of disorder, *J. Phys. A* **45**, 143001 (2012).
- [13] M. Piraud, L. Pezzé, and L. Sanchez-Palencia, Quantum transport of atomic matter waves in anisotropic two-dimensional and three-dimensional disorder, *New J. Phys.* **15**, 075007 (2013).
- [14] D. Delande and G. Orso, Mobility edge for cold atoms in laser speckle potentials, *Phys. Rev. Lett.* **113**, 060601 (2014).
- [15] L. Sanchez-Palencia, D. Clément, P. Lukan, P. Bouyer, G. V. Shlyapnikov, and A. Aspect, Anderson localization of expanding Bose-Einstein condensates in random potentials, *Phys. Rev. Lett.* **98**, 210401 (2007).
- [16] T. Giamarchi and H. J. Schulz, Anderson localization and interactions in one-dimensional metals, *Phys. Rev. B* **37**, 325 (1988).
- [17] M. P. A. Fisher, P. B. Weichman, G. Grinstein, and D. S. Fisher, Boson localization and the superfluid-insulator transition, *Phys. Rev. B* **40**, 546 (1989).
- [18] T. Geiger, A. Buchleitner, and T. Wellens, Microscopic scattering theory for interacting bosons in weak random potentials, *New J. Phys.* **15**, 115015 (2013).
- [19] T. Khellil and A. Pelster, Hartree-Fock mean-field theory for trapped dirty bosons, *J. Stat. Mech.: Theory Exp.* **2016** (6), 063301.
- [20] T. Khellil and A. Pelster, Dirty bosons in a three-dimensional harmonic trap, *J. Stat. Mech.: Theory Exp.* **2017** (9), 093108.
- [21] J. E. Lye, L. Fallani, M. Modugno, D. S. Wiersma, C. Fort, and M. Inguscio, Bose-Einstein condensate in a random potential, *Phys. Rev. Lett.* **95**, 070401 (2005).
- [22] T. Schulte, S. Drenkelforth, J. Kruse, W. Ertmer, J. Arlt, K. Sacha, J. Zakrzewski, and M. Lewenstein, Routes towards Anderson-like localization of Bose-Einstein condensates in disordered optical lattices, *Phys. Rev. Lett.* **95**, 170411 (2005).
- [23] D. Clément, P. Bouyer, A. Aspect, and L. Sanchez-Palencia, Density modulations in an elongated Bose-Einstein condensate released from a disordered potential, *Phys. Rev. A* **77**, 033631 (2008).
- [24] Y. P. Chen, J. Hitchcock, D. Dries, M. Junker, C. Welford, and R. G. Hulet, Phase coherence and superfluid-insulator transition in a disordered Bose-Einstein condensate, *Phys. Rev. A* **77**, 033632 (2008).
- [25] B. Deissler, M. Zaccanti, G. Roati, C. D'Errico, M. Fattori, M. Modugno, G. Modugno, and M. Inguscio, Delocalization of a disordered bosonic system by repulsive interactions, *Nat. Phys.* **6**, 354 (2010).
- [26] I. Guillamón, R. Córdoba, J. Sesé, J. M. De Teresa, M. R. Ibarra, S. Vieira, and H. Suderow, Enhancement of long-range correlations in a 2D vortex lattice by an incommensurate 1D disorder potential, *Nat. Phys.* **10**, 851 (2014).
- [27] A. Boissé, G. Berthet, L. Fouché, G. Salomon, A. Aspect, S. Lepoutre, and T. Bourdel, Nonlinear scattering of atomic bright solitons in disorder, *EPL* **117**, 10007 (2017).
- [28] L. Sanchez-Palencia and M. Lewenstein, Disordered quantum gases under control, *Nat. Phys.* **6**, 87 (2010).
- [29] L. Sanchez-Palencia, Smoothing effect and delocalization of interacting Bose-Einstein condensates in random potentials, *Phys. Rev. A* **74**, 053625 (2006).
- [30] T. Nattermann and V. L. Pokrovsky, Bose-Einstein condensates in strongly disordered traps, *Phys. Rev. Lett.* **100**, 060402 (2008).
- [31] E. Akkermans, S. Ghosh, and Z. H. Musslimani, Numerical study of one-dimensional and interacting Bose-Einstein condensates in a random potential, *J. Phys. B* **41**, 045302 (2008).
- [32] G. M. Falco, T. Nattermann, and V. L. Pokrovsky, Weakly interacting Bose gas in a random environment, *Phys. Rev. B* **80**, 104515 (2009).
- [33] Y. Cheng and S. K. Adhikari, Matter-wave localization in a random potential, *Phys. Rev. A* **82**, 013631 (2010).
- [34] N. Bilas and N. Pavloff, Anderson localization of elementary excitations in a one-dimensional Bose-Einstein condensate, *Eur. Phys. J. D* **40**, 387 (2006).
- [35] V. Gurarie, G. Refael, and J. T. Chalker, Excitations of one-dimensional Bose-Einstein condensates in a random potential, *Phys. Rev. Lett.* **101**, 170407 (2008).
- [36] L. Fontanesi, M. Wouters, and V. Savona, Superfluid to Bose-glass transition in a 1D weakly interacting Bose gas, *Phys. Rev. Lett.* **103**, 030403 (2009).
- [37] C. Gaul, N. Renner, and C. A. Müller, Speed of sound in disordered Bose-Einstein condensates, *Phys. Rev. A* **80**, 053620 (2009).
- [38] M. Modugno, Collective dynamics and expansion of a Bose-Einstein condensate in a random potential, *Phys. Rev. A* **73**, 013606 (2006).
- [39] S. Palpacelli and S. Succi, Quantum lattice Boltzmann simulation of expanding Bose-Einstein condensates in random potentials, *Phys. Rev. E* **77**, 066708 (2008).
- [40] C. Joshi and S. Ghosh, Density, phase and coherence properties of a low dimensional Bose-Einstein systems moving in a disordered potential, *Eur. Phys. J. B* **68**, 467 (2009).
- [41] S. Donsa, H. Hofstätter, O. Koch, J. Burgdörfer, and I. Březinová, Long-time expansion of a Bose-Einstein condensate: Observability of Anderson localization, *Phys. Rev. A* **96**, 043630 (2017).
- [42] M. S. Najafabadi, D. Schumayer, and D. A. W. Hutchinson, Effects of disorder upon transport and Anderson localization in a finite, two-dimensional Bose gas, *Phys. Rev. A* **104**, 063311 (2021).
- [43] T. Scoquart, T. Wellens, D. Delande, and N. Cherroret, Quench dynamics of a weakly interacting disordered Bose gas in momentum space, *Phys. Rev. Res.* **2**, 033349 (2020).
- [44] Scoquart, T., Larré, P.-É., Delande, D., and Cherroret, N., Weakly interacting disordered Bose gases out of equilibrium: From multiple scattering to superfluidity(a), *EPL* **132**, 66001 (2020).
- [45] N. Cherroret, T. Scoquart, and D. Delande, Coherent multiple scattering of out-of-equilibrium interacting Bose gases, *Ann. Phys.* **435**, 168543 (2021), Special Issue on Localisation 2020.

- [46] P. Lugan, D. Clément, P. Bouyer, A. Aspect, M. Lewenstein, and L. Sanchez-Palencia, Ultracold Bose gases in 1D disorder: from Lifshits glass to Bose-Einstein condensate, *Phys. Rev. Lett.* **98**, 170403 (2007).
- [47] G. E. Astrakharchik, K. V. Krutitsky, and P. Navez, Phase diagram of quasi-two-dimensional bosons in a laser-speckle potential, *Phys. Rev. A* **87**, 061601 (2013).
- [48] G. Carleo, G. Boéris, M. Holzmann, and L. Sanchez-Palencia, Universal superfluid transition and transport properties of two-dimensional dirty bosons, *Phys. Rev. Lett.* **111**, 050406 (2013).
- [49] J. Saliba, P. Lugan, and V. Savona, Superfluid-insulator transition of two-dimensional disordered Bose gases, *Phys. Rev. A* **90**, 031603 (2014).
- [50] M. Albert and C. A. Müller, Full distribution of the superfluid fraction and extreme value statistics in a one-dimensional disordered Bose gas, *Phys. Rev. A* **101**, 023605 (2020).
- [51] K. Sacha, C. A. Müller, D. Delande, and J. Zakrzewski, Anderson localization of solitons, *Phys. Rev. Lett.* **103**, 210402 (2009).
- [52] M. Płodzień and K. Sacha, Breakdown of Anderson localization of interacting quantum bright solitons in a disorder potential, *Phys. Rev. A* **86**, 033617 (2012).
- [53] M. Mochol, M. Płodzień, and K. Sacha, Dark soliton in a disorder potential, *Phys. Rev. A* **85**, 023627 (2012).
- [54] A. Aftalion, J. Dalibard, and C. Josserand, *Équation de Schrödinger non linéaire : des condensats de Bose-Einstein aux condensats de Bose-Einstein aux dispersions* (2010), Lecture notes.
- [55] M. Filoche and S. Mayboroda, Universal mechanism for Anderson and weak localization, *Proc. Natl. Aca. Sci. USA* **109**, 14761 (2012).
- [56] R. D'Agosta, B. A. Malomed, and C. Presilla, Stationary solutions of the Gross-Pitaevskii equation with linear counterpart, *Phys. Lett. A* **275**, 424 (2000).
- [57] Y. S. Kivshar, T. J. Alexander, and S. K. Turitsyn, Nonlinear modes of a macroscopic quantum oscillator, *Phys. Lett. A* **278**, 225 (2001).
- [58] D. N. Arnold, G. David, D. Jerison, S. Mayboroda, and M. Filoche, Effective confining potential of quantum states in disordered media, *Phys. Rev. Lett.* **116**, 056602 (2016).
- [59] L. Fallani, C. Fort, and M. Inguscio, Bose-Einstein condensates in disordered potentials, in *Adv. At. Mol. Opt. Phys.*, Adv. At. Mol. Opt. Phys., Vol. 56 (Academic Press, 2008) pp. 119–160.
- [60] R. Zamora-Zamora, G. A. Domínguez-Castro, C. Trallero-Giner, R. Paredes, and V. Romero-Rochín, Validity of Gross-Pitaevskii solutions of harmonically confined BEC gases in reduced dimensions, *J. Phys. Commun.* **3**, 085003 (2019).
- [61] D. Clément, A. F. Varón, J. A. Retter, L. Sanchez-Palencia, A. Aspect, and P. Bouyer, Experimental study of the transport of coherent interacting matter-waves in a 1D random potential induced by laser speckle, *New J. Phys.* **8**, 165 (2006).
- [62] R. Kuhn, *Coherent transport of matter waves in disordered optical potentials*, Ph.D. thesis, Université Nice Sophia Antipolis (2007).
- [63] D. N. Arnold, G. David, M. Filoche, D. Jerison, and S. Mayboroda, Computing spectra without solving eigenvalue problems, *SIAM J. Sci. Comp.* **41**, B69 (2019).
- [64] P. Desforges, S. Mayboroda, S. Zhang, G. David, D. N. Arnold, W. Wang, and M. Filoche, Sharp estimates for the integrated density of states in Anderson tight-binding models, *Phys. Rev. A* **104**, 012207 (2021).
- [65] P. Muruganandam and S. K. Adhikari, Fortran programs for the time-dependent Gross-Pitaevskii equation in a fully anisotropic trap, *Comput. Phys. Commun.* **180**, 1888 (2009).
- [66] J. H. Mathews, *Numerical methods for mathematics, science and engineering*, 1st ed. (Prentice Hall, Hoboken, 1991).
- [67] S. Lepoutre, L. Fouché, A. Boissé, G. Berthet, G. Salomon, A. Aspect, and T. Bourdel, Production of strongly bound ^{39}K bright solitons, *Phys. Rev. A* **94**, 053626 (2016).
- [68] L. Sanchez-Palencia, D. Clément, P. Lugan, P. Bouyer, and A. Aspect, Disorder-induced trapping versus Anderson localization in Bose-Einstein condensates expanding in disordered potentials, *New J. Phys.* **10**, 045019 (2008).
- [69] T. Kottos, F. M. Izrailev, and A. Politi, Finite-length Lyapunov exponents and conductance for quasi-1d disordered solids, *Physica D: Nonlinear Phenomena* **131**, 155 (1999).
- [70] L. D. Carr, C. W. Clark, and W. P. Reinhardt, Stationary solutions of the one-dimensional nonlinear Schrödinger equation. II. Case of attractive nonlinearity, *Phys. Rev. A* **62**, 063611 (2000).
- [71] L. D. Carr, M. A. Leung, and W. P. Reinhardt, Dynamics of the Bose-Einstein condensate: quasi-one-dimension and beyond, *J. Phys. B: At. Mol. Opt. Phys.* **33**, 3983 (2000).
- [72] R. J. Dodd, M. Edwards, C. J. Williams, C. W. Clark, M. J. Holland, P. A. Ruprecht, and K. Burnett, Role of attractive interactions on Bose-Einstein condensation, *Phys. Rev. A* **54**, 661 (1996).
- [73] G. Baym and C. J. Pethick, Ground-state properties of magnetically trapped Bose-condensed rubidium gas, *Phys. Rev. Lett.* **76**, 6 (1996).
- [74] P. Lugan, A. Aspect, L. Sanchez-Palencia, D. Delande, B. Grémaud, C. A. Müller, and C. Miniatura, One-dimensional Anderson localization in certain correlated random potentials, *Phys. Rev. A* **80**, 023605 (2009).
- [75] R. Seiringer and S. Warzel, Decay of correlations and absence of superfluidity in the disordered Tonks-Girardeau gas, *New J. Phys.* **18**, 035002 (2016).
- [76] D. N. Arnold, G. David, M. Filoche, D. Jerison, and S. Mayboroda, Localization of eigenfunctions via an effective potential, *Commun. Part. Diff. Eq.* **44**, 1186 (2019).
- [77] R. Seiringer, J. Yngvason, and V. A. Zagrebnov, Disordered Bose-Einstein condensates with interaction in one dimension, *J. Stat. Mech.* **2012**, P11007 (2012).
- [78] I. Lifshitz, Structure of the energy spectrum of impurity bands in disordered solid solutions, *Sov. Phys. JETP* **17**, 1159 (1963).
- [79] I. Lifshitz, Energy spectrum structure and quantum states of disordered condensed systems, *Sov. Phys. Usp.* **7**, 549 (1965).
- [80] J. M. Luttinger and H. K. Sy, Low-lying energy spectrum of a one-dimensional disordered system, *Phys. Rev. A* **7**, 701 (1973).
- [81] S. S. Shamailov, D. J. Brown, T. A. Haase, and M. D. Hoogerland, Computing the eigenstate localisation length at very low energies from Localisation Landscape Theory, *SciPost Phys. Core* **4**, 17 (2021).
- [82] F. M. Izrailev and A. A. Krokhin, Localization and the

- mobility edge in one-dimensional potentials with correlated disorder, *Phys. Rev. Lett.* **82**, 4062 (1999).
- [83] T. Bourdel, Phase diagrams of two-dimensional and three-dimensional disordered Bose gases in the local density approximation, *Phys. Rev. A* **86**, 063626 (2012).
- [84] J. Stasińska, P. Massignan, M. Bishop, J. Wehr, A. Sanpera, and M. Lewenstein, The glass to superfluid transition in dirty bosons on a lattice, *New J. Phys.* **14**, 043043 (2012).
- [85] A. Collin, P. Massignan, and C. J. Pethick, Energy-dependent effective interactions for dilute many-body systems, *Phys. Rev. A* **75**, 013615 (2007).
- [86] A. Cappellaro and L. Salasnich, Effective field theory of bosons with finite-range interaction in a disordered environment, *Phys. Rev. A* **101**, 053628 (2020).